UiT
THE ARCTIC
UNIVERSITY
OF NORWAY

Faculty of Science and Technology, Department of Geology

Modelling the subglacial hydrology of the former Barents Sea Ice Sheet

—

Eythor Gudlaugsson

A dissertation for the degree of Philosophiae Doctor – October 2015

Modelling the subglacial hydrology of the former Barents Sea Ice Sheet

Eythor Gudlaugsson

A dissertation for the degree of

Philosophiae Doctor

UiT / THE ARCTIC UNIVERSITY OF NORWAY

FACULTY OF SCIENCE AND TECHNOLOGY

DEPARTMENT OF GEOLOGY

OCTOBER 2015

I. PREFACE

This PhD thesis was carried out at the University of Tromsø - The Arctic University of Norway from March 2011 to October 2015. The work was mainly financed by the Trainee school in Arctic Marine Geology and Geophysics (AMGG) at the University of Tromsø as well as the Petromaks project "Glaciations in the Barents Sea area" (GlaciBar) and the Centre of Excellence "Arctic Gas Hydrate, Environment and Climate" (CAGE). Additional support was provided by the Norwegian Research School in Climate Dynamics (ResClim).

The main supervisors were Prof. Karin Andreassen at the University of Tromsø and Prof. Angelika Humbert at the Alfred Wegener Institute in Germany. Co-supervisor were Dr. Jack Kohler at the Norwegian Polar Institute and Dr. Monica Winsborrow at the University of Tromsø.

During the course of the PhD I have attended numerous workshops, courses and summer schools and had the opportunity to present my work at several international conferences around the world. I have been on a research stay in Hamburg as well as on several visits to the Alfred Wegener Institute in Germany. I have had the opportunity to join many research cruises around the Barents Sea, Svalbard and even all the way to the east coast of Greenland. In addition to cruises, duty work has included making web pages, processing scripts for multibeam and seismic data and organizing workshops and courses for colleagues at the department.

The thesis itself consists of a short introduction and three scientific papers. These are:

Paper 1

Gudlaugsson, E., Humbert, A., Winsborrow, M., and Andreassen K., (2013), Subglacial roughness of the former Barents Sea ice sheet, J. Geophys. Res. Earth Surf., 118, 25462556, doi:10.1002/2013JF002714.

Paper 2

Gudlaugsson, E., Humbert, A., Kleiner, T., Kohler, J., and Andreassen, K., (2015), The influence of a model subglacial lake on ice dynamics and internal layering, The Cryosphere Discuss., 9, 3859-3886, doi:10.5194/tcd-9-3859-2015.

Paper 3

Gudlaugsson, E., Humbert, A., Andreassen, K., Clason, C., Kleiner, T. and Beyer, S.: Eurasian ice sheet dynamics and sensitivity to subglacial hydrology. Manuscript

II. ACKNOWLEDGEMENTS

First and foremost I would like to thank my two main supervisors, Karin and Angelika for all their excellent advice, help and patience. Without their support and inspiration I never would have made it this far. I would also like to thank my two co-supervisors Jack and Monica for being there for me whenever I needed it.

Special thanks go to Thomas Kleiner, who although not officially one of my supervisors, has certainly supported me the whole way and provided me with invaluable assistance and advice.

I would also like to thank my friends and colleagues at the University of Tromsø for all the good times throughout the years, the glaciology group at the AWI for putting up with me during all those visits, the support group at STALLO/NOTUR, Rolf the computer expert and my former colleagues in Hamburg, Martin and Nina.

Last but not least I would like to thank my family, fiancée and close friends for being there for me during all those years and for assuring me that the world is round whenever I felt like I was falling off the edge.

Takk kærlega!

""Now look, your grace," said Sancho, "what you see over there
aren't giants, but windmills, and what seems to be arms are
just their sails, that go around in the wind and turn the millstone."
"Obviously," replied Don Quixote, "you don't know much about adventures.""

- Miguel de Cervantes Saavedra, Don Quixote

TABLE OF CONTENTS

IV. INTRODUCTION

Today's polar ice sheets hold enough ice to raise the current sea levels by around 70 m were they to completely disintegrate. At the last glacial maximum (LGM), roughly 20-25 ka years ago, ice covered not only Antarctica and Greenland as it does today but also large parts of the Eurasian and North American Arctic (Clark and Mix 2002). The extent of the worlds ice cover is mainly governed by climate and climate is influenced by the amount of sunlight reaching earth. Large ice sheets affect the earths radiation balance and freshwater flux to the ocean and can have a strong influence on their own climate and surrounding ocean currents (Clark et al. 1999). In recent decades it has emerged that humans can also have a strong influence on climate (Oreskes 2004), where emissions of greenhouse gases and deforestation among other things have caused global temperatures to rise and a disruption of typical weather patterns. Since the industrial revolution, global temperatures on earth have risen fast in a historical perspective or about 1°C in total (Stocker et al. 2014). This is causing the worlds ice sheets to melt and sea level to rise. As ocean temperatures rise, they expand and roughly 50% of today's annual increase in sea level is due to expanding oceans, whereas the other half comes from increased melt from mountain glaciers and ice sheets (Stocker et al. 2014). Predicting how much and how fast ice will melt with a warming climate remains a considerable challenge. Surface accumulation is balanced by melt and direct output of ice to the worlds oceans. Some of the most important processes affecting the flow of ice take place at the interface between the ice and the underlying bed, which is almost impossible to access (Clarke 2005). We therefore have to rely on very sparse, indirect, often remotely measured quantities to infer characteristics of the subglacial systems of modern-day ice sheets. An alternative is to study the history of past ice sheets and the geological evidence that they leave behind as they disintegrate. This has the benefit of complete, direct access to the former subglacial interface between the ice and the underlying substrate which can thus be surveyed in much closer detail. Geological and geophysical data can then be tied together with numerical models, and hypotheses of how subglacial processes take place put to the test.

Subglacial processes

Ice flows due to the actions of gravity on its own mass. At high pressures (roughly 50m depth/overburden) ice starts to behave like a fluid, viscously deforming under its own weight. This internal deformation creates heat within the ice, which along with the geothermal heat flux from below can cause ice to reach melting temperatures at its base. Ice at pressure melting temperatures is typically found underneath very thick ice, due to its poor conductive abilities, or in areas of fast flow, so called ice streams (Siegert et al. 1996). When ice reaches pressure melting, it looses its strong adhesive bond to the ground and can start to slide at it's base, adding frictional heating to the energy balance. Any surplus in energy that can not be transported away, leads to production of melt water. The presence of water drastically alters the dynamics of ice flow, causing basal velocities to increase, whereas internal deformation typically decreases due to the lower basal resistance. Basal water moves rapidly compared to the overlying ice, from areas of high pressure potential to areas with lower potential and can flow both in thin films or a network of connected cavities (Lliboutry 1968, Weertman 1972). Once water velocities reach a certain threshold, the turbulent energy of the flowing water can melt a channel which both alters the surrounding pressure potential and allows the water to quickly gain speed as it passes through the subglacial hydrological system (Flowers 2015).

Whereas surface water flowing on land is governed by the shape of the earth's surface, the flow of subglacial water is governed by a similar but fictitious surface, one that takes into account not just the differences in water levels but also differences in ice thickness. This means that the flow of subglacial water is dictated not only by bedrock gradients but also by gradients of the ice surface, where the surface gradients are roughly 10 times more important then that bedrock ones (Le Brocq et al. 2009, Röthlisberger 1972). Subglacial water is capable of flowing uphill, along gradients of positive slope, if the surface gradients permit. As with surface lakes, water can pond in areas of minima in this fictitious pressure potential surface. Once a subglacial lake has formed it has a profound influence on ice dynamics. Subglacial lakes in Antarctica have been shown to both increase ice velocities as well as affecting the basal thermal regime (Bell et al. 2007).

The flow of ice is ultimately resisted solely at its base and sides. The base consists of protruding elements of various sizes, rocks, hills and alike (Kamb 1970). If the ice is frozen

to the base, then there is generally no relative movement between the ice and the ground and ice velocities approach zero at the base. When the ice reaches melting temperatures it starts to slide and has to overcome any obstacles in its path. Ice moves across the base either by regelation, whereby the enhanced pressure on the upstream side of an obstacle depresses the melting point, allowing the water to momentarily melt, flow around the obstacle and then refreeze on the lee side where the pressure drops again (Weertman 1957). This process is limited by the rate of heat exchange between the upstream and the downstream side through the obstacle, and thus only efficient for small obstacles, typically in the range of a few centimeters. For larger obstacles, the ice moves around them through a process known as enhanced creep, where the enhanced pressure on the upstream side of obstacles decreases the viscosity of ice, which depends on both effective pressure, temperature and water content, allowing it to flow more easily around obstacles of greater size than with regelation. In general, the majority of resistance offered by the bed on the flow of ice is considered to arise from larger obstacles, through enhanced creep (Gudmundsson 1997). By assuming a bed consisting of superimposed sinusoids Nye (1970), concluded that the resistance that a bed offers is at a maximum when the obstacle size is large enough and small enough for both of these two processes to be inefficient and he called this the controlling obstacle size. Typically, it is considered to be around 10cm. Roughness of that order is therefore of great significance for glacier sliding. Not many basal datasets of modern ice sheets have such high resolution though, but roughness on larger spatial scales can still give valuable insights into the dynamics and history of ice sheets and land evolution (Bingham and Siegert 2009).

Basal sliding

The original motivation for studying subglacial roughness came from the study of subglacial sliding (Weertman 1957). The way that both roughness and subglacial water ultimately influence ice dynamics is through basal sliding. Roughness affects the speed at which ice slides over terrain with rough surfaces leading to higher traction and slower ice flow. This picture is somewhat complicated by the fact that both higher traction and faster basal velocities typically increase meltwater production leading to more available water underneath the ice and a reduction in basal friction. The presence of pressurized water at the base (due to ice overburden), separates the ice from the underlying sediments or bedrock and effectively drowns out the small scale roughness elements, obstacles of smaller size than the thickness of the water layer (Johnson and Fastook 2002). Pressurized basal water also penetrates the sediments, separating sediment particles from one another, drastically reducing its shear strength and making it easier for the sediment to deform (Tulaczyk et al. 2000). A thick water layer and high water pressures thus reduce the amount of frictional resistance that the base can offer and consequently increase ice velocities.

Study area

The main study area is the Barents Sea (BS), where the former Barents Sea Ice Sheet (BSIS) resided during the last glacial cycle (Clason et al. 2014). Modelling the BSIS alone is not feasible though as the Fennoscandian Ice Sheet and the BSIS united and affected each other through both merging ice flow and isostatic adjustment, not to mention any dynamic influences on climate that they may have had as this is typically not accounted for in numerical ice sheet models. The BS covers one of the widest continental shelves in the world, comparable in size to the one covered by the West Antarctic Ice Sheet (WAIS) today. The shelf is scarred with many glacial troughs where large ice streams were active in the past. The largest of these is the Bjornoyrenna Trough (Andreassen and Winsborrow 2009). Bjornoyrenna contains several grounding zone wedges that indicate stepwise retreat and readvance during the last deglaciation as well as areas covered with megascale glacial lineations (MSGLs), indicative of fast streaming flow (Andreassen et al. 2014, Winsborrow et al. 2010). Deglaciation was thus much more dynamic than previously thought. Trough mouth fans hold sediment archives of erosional history through the ages (Laberg et al. 2012) and extensive subglacial channels indicate that subglacial water played a significant role in the ice sheets demise (Bjarnadóttir et al. 2014). A known drumlin field can also be found in northern Bjornoyrenna, so the former ice stream can be considered to be of wide interest and importance for a variety of reasons.

The Barents Sea itself is characterized by shallow banks with water depths of 100-200m, and water depths of up to 500-600m in the deepest parts of the troughs. It contains a Quaternary sediment sequence of up to 300m in thickness with a thin postglacial veneer of Holocene sediments of up to 2m (Elverhøi and Solheim 1983, Vorren et al. 1988).

During glacial times, the BS ice cover was similar in extent and thickness as the current WAIS and thus offers a good geological analog to it. Large parts of the ice sheet would have been below sea level, resting on a combination of marine and glacial sediments and during the LGM the ice sheet is thought to have extended all the way to the shelf edge (Anderson et al. 2002, Evans et al. 2006, Svendsen et al. 2004).

Study aim

The overall aim of this thesis is to investigate subglacial processes of the former Barents Sea Ice Sheet and to estimate their relative importance. We do this by applying numerical models and procedures and by comparing their output with empirical evidence left behind by the former ice sheet. In particular, we address the following questions:

- How does subglacial roughness vary spatially in the Barents Sea area and what can be said about the glacial history based on the distribution of rough and smooth areas?
- How was the evolution of the ice sheet affected by the presence of water at the base?
- How does the presence of a subglacial lake affect the thermodynamics of the overlying ice?
- Can past drainage of subglacial lakes be detected from looking at internal layers within the ice?
- How is subglacial roughness related to glacial erosion and what are the important temporal and spatial scales?

V. SUMMARY OF PAPERS

Paper 1

Gudlaugsson, E., Humbert, A., Winsborrow, M., and Andreassen, K., (2013), Subglacial roughness of the former Barents Sea ice sheet, J. Geophys. Res. Earth Surf., 118, 25462556, doi:10.1002/2013JF002714.

Here, we use a 750 km long, single trackline of high resolution multibeam bathymetric data ($\sim 12\,m$), tracing the whole length of a major past ice stream as well as a composite dataset ($\sim 600\,m$) to investigate the subglacial roughness of the former Barents Sea Ice Sheet. The composite dataset consists of multibeam, seismic and sonar data and covers the whole South-Western Barents Sea. Similiar roughness studies of glaciated areas in either Greenland or Antarctica often suffer from very limited data coverage and low resolution, whereas the Barents Sea is one of the best covered in the world. This offered the possibility of studying the effect of varying the profile length, resolution and orientation used in the roughness calculation, as well as spatial variability of the roughness estimate. We found that the roughness estimate shows little dependence on profile resolution as long as the profile length is kept constant and a certain minimum of datapoints are used. It shows higher dependence on both orientation and profile length, keeping the number of datapoints fixed. Glacial geomorphological features show a characteristic roughness signal indicating that they could potentially be identified solely based on their wavelength composition. Additionally, as roughness is typically reduced preferentially in flow directions, past flow directions can to some degree be reconstructed based on the orientation dependence of roughness.

Paper 2

Gudlaugsson, E., Humbert, A., Kleiner, T., Kohler, J., and Andreassen, K., (2015), The influence of a model subglacial lake on ice dynamics and internal layering, The Cryosphere Discuss., 9, 3859-3886, doi:10.5194/tcd-9-3859-2015.

Many subglacial lakes have been identified in Antarctica and a few, recently, in Greenland as well. This paper explores the influence of a subglacial lake on ice dynamics and internal layers by means of numerical modelling as well as simulating the effect of a subglacial drainage event on isochrones. We provide an explanation for characteristic dip and

ridge features found at the edges of many subglacial lakes and conclude that draining lakes can result in travelling waves at depth within isochrones, thus indicating the possibility of detecting past drainage events with ice penetrating radar. Subglacial lakes represent areas of the ice sheet incapable of exerting any shear stress on the overlying ice and in the transition zone from little to full slip at lake edges, stresses are concentrated over a small area which both releases deformational energy as well as decreases the ice viscosity locally. Ice over the lake itself, moves more like in an ice shelf with uniform velocity and zero shear at the base. Dip and ridge features are controlled by the decrease in ice viscosity with depth, as the lower layers support less horizontal and longitudinal stress than the stiffer ice above subglacial lakes. Due to the limited vertical extent, a dip on the upstream side and a ridge on the downstream side are produced.

Paper 3

Gudlaugsson, E., Humbert, A., Andreassen, K., Clason, C., Kleiner, T. and Beyer, S.: Eurasian ice sheet dynamics and sensitivity to subglacial hydrology. Manuscript

Recent studies have indicated that subglacial hydrology played an important role in the relatively fast disintegration of the former Barents Sea ice sheet. In this paper we investigate the effect of subglacial water on the evolution of the Barents Sea and the Fennoscandian Ice Sheets by implementing a thin film model of water flow into and existing numerical ice sheet model (SICOPOLIS). Focusing on the last glacial cycle we find that coupling the thickness of the water film to subglacial sliding not only results in increased sliding but also lower ice volume building up over time. The fraction of the ice sheet base at pressure melting is reduced as ice thickness drops and vertical flow of cold ice towards the base increases. We use sinks in the hydrological potential as indications for past locations of subglacial lakes and present a probability distribution of lake existence, based on their depth and longevity. Lake volume follows dynamic changes in the ice sheet geometry and thermal regime and during deglaciation phases a strong decrease in estimated volume is shown, indicating a strong increase in output of subglacial water towards the margin.

VI. SYNTHESIS

This study focuses on subglacial processes of the former Barents Sea Ice Sheet. We perform a spectral analysis of the former ice/bed interface and run numerical simulations of the ice sheet evolution (both the Fennoscandian and the Barents Sea Ice Sheets) during the last glacial cycle, incorporating a simple representation of the subglacial hydrological system. In addition, we employ a Full-Stokes finite element model to investigate the influence of a subglacial lake on ice dynamics and internal layers.

We have shown that there is a high degree of variability in spectral roughness across the Barents Sea (paper 1). Troughs are typically characterized by low roughness on all scales whereas areas that have endured less glacial erosion such as Spitzbergenbanken and others are rougher. Values compare well with what has been estimated for similar areas in Antarctica (i.e. Bingham and Siegert (2009)). Our work thus comprises the first steps in quantitatively comparing a currently ice covered and a previously ice covered area. Such roughness studies provide an interesting mechanism to relate deglaciated areas to their glaciated counterparts in either Antarctica or Greenland. By comparing roughness characteristics we can thus possibly extract more information about the subglacial conditions and past ice dynamics of deglaciated areas than otherwise possible. In addition, surfaces have been shown to have a memory of past ice flow directions but work still remains on determining how roughness of different spatial scales relates to rates of basal erosion and the temporal evolution of glacial landscapes.

Along with roughness, bed composition and type, the resistance that a glacier bed can offer depends on the thermal conditions at the base. Temperate ice is often underlain by subglacial water which greatly affects flow. Past modelling studies of the Fennoscandian and Barents Sea Ice Sheets have typically not included the effects of subglacial hydrology as little was known about its importance. Several recent studies (Bjarnadóttir et al. 2014, Winsborrow et al. 2010) have indicated its significance on glacial dynamics in the region and especially on the most recent deglaciation phase of the ice sheets. In paper 3 we implemented a simple representation of subglacial hydrology into an exisiting ice sheet model and ran simulations of the Fennoscandian/Barents Sea ice sheets. Hydrology coupled (HC) sliding leads to increased basal velocities and a lower ice volume building up over time. When HC sliding is included, a considerably smaller part of the ice sheets base is at pressure melting

due to the increased vertical flow of colder ice from above and less available deformational energy. Subglacial hydrology has been shown to not only enhance basal velocity but also to be a potential driver of dynamic changes in ice stream configuration. Shutdown of ice stream C (Anandakrishnan and Alley 1997) has been attributed to so called water-piracy, where changes in surface geometry have caused meltwater to alternate its route down to the margin, drastically affecting ice streaming in the area. Modelling studies with simplified ice physics, highly smoothed bathymetry or very coarse resolution are unlikely to result in such dynamic behaviour though, as the water layer distribution is also smoothed out. Several subglacial lakes have been predicted to have existed in the Fennoscandian/Barents Sea area, several of which currently exist as surface lakes in Scandinavia. This has implications for future geological studies of subglacial lakes in the region. The best candidates for exploration, considering ease of access and probability of existence, are probably those predicted over mainland Scandinavia. Many lakes that potentially existed in the Barents Sea were likely so called 'active' lakes with fast circulation of water. Drainage would likely have been reoccurring and cyclic, where the ice sheets base potentially came in and out of contact with the underlying bed, thus complicating retrieval of high quality lake sediment cores. Sediment cores from subglacial lakes are likely to hold valuable information about the past health of the subglacial system and for subglacial lakes in Antarctica, sediment cores could even potentially be used to extend palaeoenvironmental results beyond that what ice cores typically record (Bentley et al. 2013). By estimating total lake volume for the whole region and its evolution during a part of the glacial cycle we can ascertain the importance of not only taking into account subglacial flow of water but also the importance of taking into account storage of subglacial water as during rapid changes in ice sheet geometry the amount of mobile subglacial water is predicted to drastically increase as subglacial lakes drain and reduce their storage capacity. This has the potential to significantly affect ice streaming during deglaciation although a more physically realistic model would be needed to properly assess its importance.

Subglacial lakes have been shown to have a strong effect on ice dynamics (paper 2). By taking into account all stress components as well as the influence of water content on ice viscosity we established that the intense stress concentrations at the edges of subglacial lakes can reach levels high enough to induce grain-boundary melting of ice crystals and the formation of a temperate layer with a non-zero water content in the transition zone between

full sliding over the lake and less sliding either leading up to the lake or downstream of it. The characteristic dip and ridge features often seen at the edges of subglacial lakes (Bell 2008) seem to be controlled, mostly by softening of ice with depth due to increasing temperature and pressure. Drainage of subglacial lakes leaves a trace in internal layers which implies that it might be possible to identify past drainage events from combined studies of radio-echo sounding/isochrones and numerical modelling. The drainage history of lakes where a strong signal is recorded could thus be deciphered back in time, although varying basal conditions and rheology downstream of the lake would impose limits on how long such a signal would be discernible. Lakes have been hypothesized to potentially being able to initiate ice streaming and to modulate ice velocity and subglacial water fluxes, although we have not been able to address those questions here. Future modelling efforts will have to work towards a complete coverage of the hydrological system, including dynamic water storage in lakes and sediment and the inclusion of channels and their effect on the hydrological potential in order to fully understand how ice dynamics are affected by the presence of water at the base.

VII. FUTURE RESEARCH

Possibilities for future research in the Barents Sea / Fennoscandian area include adopting a higher order numerical ice sheet model and coupling it to a model of land evolution, involving processes such as glacial erosion and sediment transport. The Barents Sea area is ideal for such a study as constraints on both sediment volume, removed from the shelf during glaciation periods, and sediment origin exist as the geology of the Barents Sea is relatively well studied (Laberg et al. 2012). Sediment removed from the shelf has been collected in so called trough mouth fans (TMFs) where many former ice streams crossed the shelf break. These are typically segmented and it is possible to distinguish and associate the different segments to their respective glaciation periods (Vorren and Laberg 1997), thus providing a volume estimate of discharged sediment at each outlet.

The roughness analysis, presented in paper 1, could be extended to include the whole ice covered area of the Eurasian IS during the LGM. The fact that roughness is typically smallest in the flow direction opens up possibilities of comparing roughness minima with results obtained from numerical experiments, such as glacial erosion or alike and to possibly relate the length scales of roughness to the temporal scales of glacial erosion. We have shown that certain geomorphological features can to some degree be identified based on their characteristic roughness signals and further work could provide a closer link between different features and their characteristic signal. Features such as mega scale glacial lineations and others could thus be hypothesized to exist under thick ice with relatively little data if their roughness signals in along-flow and across-flow directions match those obtained in deglaciated areas. Likewise, parallels could be drawn between basal conditions of currently ice covered areas and deglaciated ones based on roughness signatures, providing added information about past basal conditions of deglaciated areas.

The subglacial lake study (paper 2) could be extended by allowing the lake floor to move in the vertical as well as the horizontal and by including some representation of subglacial hydrology. Different boundary conditions for the inlet and the outlet (non periodic) would make it possible to examine the effect of growing the lake in order to test the hypothesis that a subglacial lake could actually initiate and maintain ice streaming. A more detailed description of the thermodynamic boundary between lake water and ice could allow for ice accretion and thus more closely resemble real lakes. This would allow latent heat to warm up the ice from below and help to explain how subglacial lakes and ice streams interact.

VIII. REFERENCES

S. Anandakrishnan and R.B. Alley. Stagnation of ice stream C, West Antarctica by water piracy. *Geophysical Research Letters*, 24(3):265–268, 1997.

J.B. Anderson, S.S. Shipp, A.L. Lowe, J.S. Wellner, and A.B. Mosola. The Antarctic ice sheet during the Last Glacial Maximum and its subsequent retreat history: a review. *Quaternary Science Reviews*, 21(1):49–70, 2002.

K. Andreassen and M. Winsborrow. Signature of ice streaming in Bjornoyrenna, Polar North Atlantic, through the Pleistocene and implications for ice-stream dynamics. *Annals Of Glaciology*, 50(52):17–26, 2009. URL `http://www.ingentaconnect.com/content/igsoc/agl/2009/00000050/00000052/art00003`.

K. Andreassen, M. Winsborrow, L.R. Bjarnadóttir, and D.C. Rüther. Ice stream retreat dynamics inferred from an assemblage of landforms in the northern Barents Sea. *Quaternary Science Reviews*, 92:246–257, 2014.

R.E. Bell. The role of subglacial water in ice-sheet mass balance. *Nature Geoscience*, 1(5):297–304, 2008.

R.E. Bell, M. Studinger, C.A. Shuman, M.A. Fahnestock, and I. Joughin. Large subglacial lakes in East Antarctica at the onset of fast-flowing ice streams. *Nature*, 445(7130):904–907, 2007.

M.J. Bentley, P. Christoffersen, D.A. Hodgson, A.M. Smith, S. Tulaczyk, and A.M. Le Brocq. *Subglacial Lake Sediments and Sedimentary Processes: Potential Archives of Ice Sheet Evolution, Past Environmental Change, and the Presence Of Life*, pages 83–110. American Geophysical Union, 2013. ISBN 9781118670354. doi: 10.1002/9781118670354.ch6. URL `http://dx.doi.org/10.1002/9781118670354.ch6`.

R.G. Bingham and M.J. Siegert. Quantifying subglacial bed roughness in Antarctica: implications for ice-sheet dynamics and history. *Quaternary Science Reviews*, 28(3-4):223–236, 2009. URL `http://dx.doi.org/10.1016/j.quascirev.2008.10.014`.

L.R. Bjarnadóttir, M. Winsborrow, and K. Andreassen. Deglaciation of the central Barents Sea. *Quaternary Science Reviews*, 92:208–226, 2014.

P.U. Clark and A.C. Mix. Ice sheets and sea level of the Last Glacial Maximum. *Quaternary Science Reviews*, 21(1):1–7, 2002.

P.U. Clark, R.B. Alley, and D. Pollard. Northern hemisphere ice-sheet influences on global climate

change. *Science*, 286(5442):1104–1111, 1999.

G.K.C. Clarke. Subglacial processes. *Annu. Rev. Earth Planet. Sci.*, 33:247–276, 2005.

C.C. Clason, P.J. Applegate, and P. Holmlund. Modelling Late Weichselian evolution of the Eurasian ice sheets forced by surface meltwater-enhanced basal sliding. *Journal of Glaciology*, 60(219):29–40, 2014.

A. Elverhøi and A. Solheim. The Barents Sea ice sheet-a sedimentological discussion. *Polar Research*, 1(1):23–42, 1983.

J. Evans, J.A. Dowdeswell, C. Ó Cofaigh, T.J. Benham, and J.B. Anderson. Extent and dynamics of the West Antarctic Ice Sheet on the outer continental shelf of Pine Island Bay during the last glaciation. *Marine Geology*, 230(1):53–72, 2006.

G.E. Flowers. Modelling water flow under glaciers and ice sheets. *Proceedings of the Royal Society of London A: Mathematical, Physical and Engineering Sciences*, 471(2176), 2015. ISSN 1364-5021. doi: 10.1098/rspa.2014.0907.

G. H. Gudmundsson. Basal-flow characteristics of a non-linear flow sliding frictionless over strongly undulating bedrock. *Journal of Glaciology*, 43(143):80–89, 1997.

J. Johnson and J.L. Fastook. Northern Hemisphere glaciation and its sensitivity to basal melt water. *Quaternary International*, 95:65–74, 2002.

B. Kamb. Sliding motion of glaciers: theory and observation. *Reviews of Geophysics*, 8(4):673–728, 1970.

J.S. Laberg, K. Andreassen, and T.O. Vorren. Late Cenozoic erosion of the high-latitude southwestern Barents Sea shelf revisited. *Geological Society of America Bulletin*, 124(1-2):77–88, 2012.

A.M. Le Brocq, A.J. Payne, M.J. Siegert, and R.B. Alley. A subglacial water-flow model for West Antarctica. *Journal of Glaciology*, 55(193):879–888, 2009.

L. Lliboutry. General theory of subglacial cavitation and sliding of temperate glaciers. *Journal of Glaciology*, 7:21–58, 1968.

J. F. Nye. Glacier sliding without cavitation in a linear viscous approximation. *Proceedings of the Royal Society of London. A. Mathematical and Physical Sciences*, 315(1522):381–403, 1970.

N. Oreskes. The scientific consensus on climate change. *Science*, 306(5702):1686–1686, 2004.

H. Röthlisberger. Water pressure in intra- and subglacial channels. *Journal of Glaciology*, 11: 177–203, 1972.

M.J. Siegert, J.A. Dowdeswell, M.R. Gorman, and N.F. McIntyre. An inventory of Antarctic sub-glacial lakes. *Antarctic Science*, 8(03):281–286, 1996.

T. Stocker, D. Qin, G. Plattner, M. Tignor, S.K. Allen, J. Boschung, A. Nauels, Y. Xia, V. Bex, and P.M. Midgley. *Climate change 2013: The physical science basis*. Cambridge University Press Cambridge, UK, and New York, 2014.

J.I. Svendsen, V. Gataullin, J. Mangerud, and L. Polyak. The glacial history of the Barents and Kara Sea region. *Developments in Quaternary Sciences*, 2:369–378, 2004.

S. Tulaczyk, W.B. Kamb, and H.F. Engelhardt. Basal mechanics of Ice Stream B, West Antarctica: 2. Undrained plastic bed model. *Journal of Geophysical Research B*, 105(B1):483–494, 2000.

T.O. Vorren and J.S. Laberg. Trough mouth fans - palaeoclimate and ice-sheet monitors. *Quaternary Science Reviews*, 16(8):865–881, 1997.

T.O. Vorren, M. Hald, and E. Lebesbye. Late Cenozoic environments in the Barents Sea. *Paleoceanography*, 3(5):601–612, 1988.

J. Weertman. On the sliding of glaciers. *J. Glaciol*, 3(21):33–38, 1957.

J. Weertman. General theory of water flow at the base of a glacier or ice sheet. *Reviews of Geophysics*, 10(1):287–333, 1972. ISSN 1944-9208. doi: 10.1029/RG010i001p00287. URL `http://dx.doi.org/10.1029/RG010i001p00287`.

M. Winsborrow, K. Andreassen, G.D. Corner, and J.S. Laberg. Deglaciation of a marine-based ice sheet: Late Weichselian palaeo-ice dynamics and retreat in the southern Barents Sea reconstructed from onshore and offshore glacial geomorphology. *Quaternary Science Reviews*, 29(3): 424–442, 2010.

Paper 1

Gudlaugsson, E., Humbert, A., Winsborrow, M., and Andreassen, K., (2013), Subglacial roughness of the former Barents Sea ice sheet, J. Geophys. Res. Earth Surf., 118, 25462556, doi:10.1002/2013JF002714.

UiT / THE ARCTIC UNIVERSITY OF NORWAY

JOURNAL OF GEOPHYSICAL RESEARCH: EARTH SURFACE, VOL. 118, 2546–2556, doi:10.1002/2013JF002714, 2013

Subglacial roughness of the former Barents Sea ice sheet

E. Gudlaugsson,[1] A. Humbert,[2] M. Winsborrow,[3] and K. Andreassen[1,4]

Received 13 January 2013; revised 12 November 2013; accepted 18 November 2013; published 20 December 2013.

[1] The roughness of a glacier bed has high importance for the estimation of the sliding velocity and can also provide valuable insights into the dynamics and history of ice sheets, depending on scale. Measurement of basal properties in present-day ice sheets is restricted to ground-penetrating radar and seismics, with surveys retrieving relatively coarse data sets. Deglaciated areas, like the Barents Sea, can be surveyed by shipborne 2-D and 3-D seismics and multibeam sonar and provide the possibility of studying the basal roughness of former ice sheets and ice streams with high resolution. Here, for the first time, we quantify the subglacial roughness of the former Barents Sea ice sheet by estimating the spectral roughness of the basal topography. We also make deductions about the past flow directions by investigating how the roughness varies along a 2-D line as the orientation of the line changes. Lastly, we investigate how the estimated basal roughness is affected by the resolution of the basal topography data set by comparing the spectral roughness along a cross section using various sampling intervals. We find that the roughness typically varies on a similar scale as for other previously marine-inundated areas in West Antarctica, with subglacial troughs having very low roughness, consistent with fast ice flow and high rates of basal erosion. The resolution of the data set seems to be of minor importance when comparing roughness indices calculated with a fixed profile length. A strong dependence on track orientation is shown for all wavelengths, with profiles having higher roughness across former flow directions than along them.

Citation: Gudlaugsson, E., A. Humbert, M. Winsborrow, and K. Andreassen (2013), Subglacial roughness of the former Barents Sea ice sheet, *J. Geophys. Res. Earth Surf.*, *118*, 2546–2556, doi:10.1002/2013JF002714.

1. Introduction

[2] The motion of ice sheets and glaciers is resisted by forces acting at the base of the ice. The degree of coupling between the bed and the ice is controlled by bed roughness and subglacial water pressure. At relatively small vertical scales, (approximately $<1m$), bed roughness is an important parameter for the estimation of the sliding velocity. At larger scales (approximately $>1m$), it can give important insights into the dynamics and history of ice sheets [*Bingham and Siegert*, 2009] and potentially be a valuable tool in identification and analysis of subglacial bed forms.

[3] The study of subglacial roughness was originally motivated by the study of subglacial sliding, which dates back to 1957 when *Weertman* [1957] proposed a two-mechanism theory for subglacial sliding. According to Weertman, basal ice at the pressure melting point moves either by regelation or by enhanced creep where the ice deforms plastically around obstacles in its path. These two mechanisms operate at different length scales, regelation operating more efficiently at the submeter scale and enhanced creep at the suprameter scale. *Kamb* [1970] and *Nye* [1970] built on his theory and, assuming a bed geometry comprising of superimposed sinusoids, included a continuous spectrum of obstacle sizes as opposed to the discrete one assumed in Weertman's analysis. They concluded that the roughness of a glacier bed could be described in terms of the power spectrum of the bed elevation. Both studies concluded that a certain controlling obstacle size exists where erosion is at a maximum and sliding velocity at a minimum, typically on the order of tens of centimeters. *Fowler* [1979, 1981] and later *Gudmundsson* [1997a, 1997b] suggested that for large-scale flow, regelation could be ignored and that most of the resistance to the flow came from larger obstacles through enhanced creep.

[4] One of the first studies ever published on the spectral roughness of a glacier bed and also the only study ever to have used data measured directly on the ground was made by *Hubbard et al.* [2000]. They combined measurements with a microroughness meter and an electro-optical distance meter to generate composite roughness spectra over almost 5 orders of magnitude in the frequency domain. Following the theoretical analysis of Nye, they defined their total roughness index as the integral of the raw power spectra over the wave numbers. *Taylor et al.* [2004] followed by outlining

[1]Department of Geology, University of Tromsø, Tromsø, Norway.
[2]Section of Glaciology, Alfred Wegener Institute Helmholtz Center for Polar and Marine Research, Bremerhaven, Germany.
[3]Statoil ASA, Harstad, Norway.
[4]Centre of Excellence for Arctic Gas Hydrate, Environment and Climate, University of Tromsø, Tromsø, Norway.

Corresponding author: E. Gudlaugsson, Department of Geology, University of Tromsø, Dramsveien 201, NO-9037 Tromsø, Norway. (eythor.gudlaugsson@uit.no)

2169-9003/13/10.1002/2013JF002714

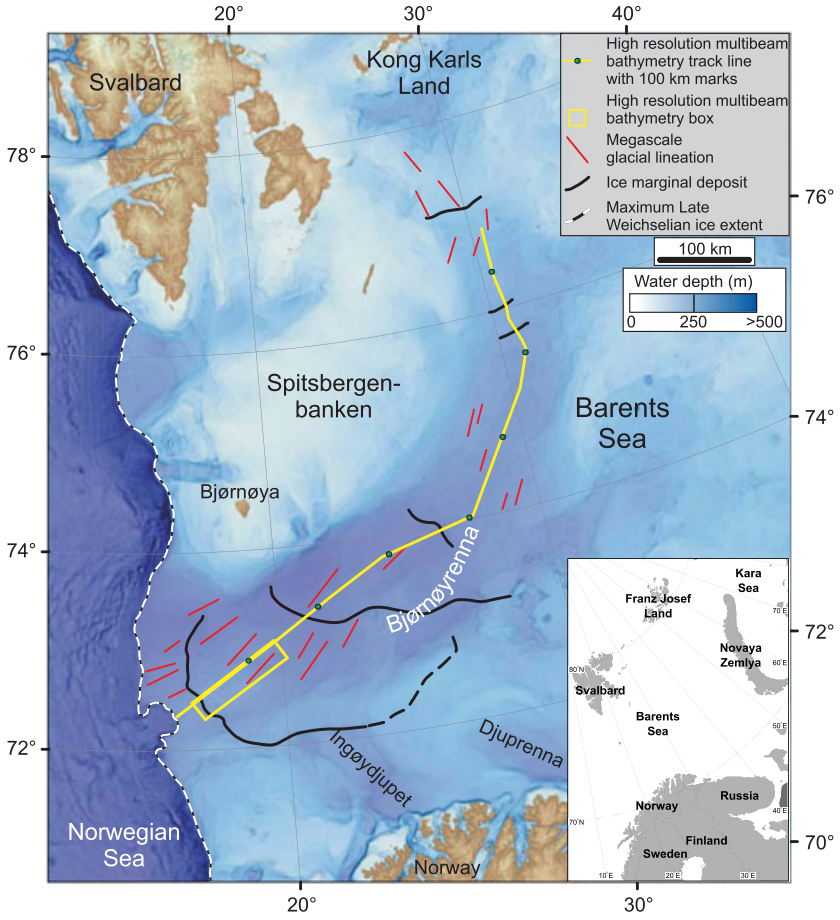

Figure 1. Bathymetry of the Barents Sea with identified ice-marginal deposits (black solid lines) and mega-scale glacial lineations (red solid lines) from *Winsborrow et al.* [2010]. Locations of high-resolution multibeam data used in this paper are indicated by yellow lines with green dots representing locations of the 100 km marks in subsequent line plots. The maximum Late Weichselian ice extent [*Svendsen et al.*, 2004b] is marked with a white stippled line. Black and white inset shows the broader location of the Barents Sea.

a general method for estimating the spectral roughness of any bed beneath an ice mass. Their method applies to any geophysical survey with topographic data, allowing comparison between different studies as long as the methodological parameters remain the same.

[5] Several authors have applied spectral roughness analysis to various sites in Antarctica, using radio echo sounding (RES) data. *Siegert et al.* [2005] correlated bed roughness with ice temperature at the base of Ridge B, Dome A, and Dome C in Antarctica, noting that beds which are rough at all scales tend to be overlain by ice which is frozen to the bed. *Bingham and Siegert* [2009] correlated low basal roughness for previously marine-inundated areas of the bed beneath the West Antarctic ice sheet (WAIS), with the presence of weak marine sediments facilitating ice flow. *Rippin et al.* [2011] investigated the relationship between ice velocity and basal roughness for Pine Island Glacier and also correlated smooth areas with deposits of marine sediments.

[6] Analyses of bed roughness offer the exciting potential to quantitatively compare contemporary subglacial landscapes and Quaternary glaciated landscapes, an important tool in improving our understanding of landscape evolution and glacial thermal regimes. As a contribution toward such work, this paper presents results from the first study of continental scale bed roughness across a Quaternary glaciated landscape: the bed of the former Barents Sea ice sheet (BSIS). As opposed to the RES data sets used in most previous studies, this study uses seismic and multibeam bathymetric data sets. The greater data coverage and better resolution of such data sets provide a unique opportunity to investigate roughness over a much larger part of the bed, across a wider range of scales and range of orientations relative to ice flow direction. In addition to characterizing the bed roughness of the BSIS, we investigate the impact of varying the resolution and the moving window length on the calculated roughness, as well as examining the effect of varying track orientations, something which is not possible with RES data sets from contemporary ice sheets. Varying track orientations allows for a rough estimation of former flow directions. In previous work, estimation of the angle dependence has been restricted to differences in roughness at track line crossover points, whereas our data set allows us to extract roughness along all directions. In comparing our results of a Quaternary glaciated landscape to the results of similar analyses done for modern subglacial environments in Antarctica, we are able to draw conclusions

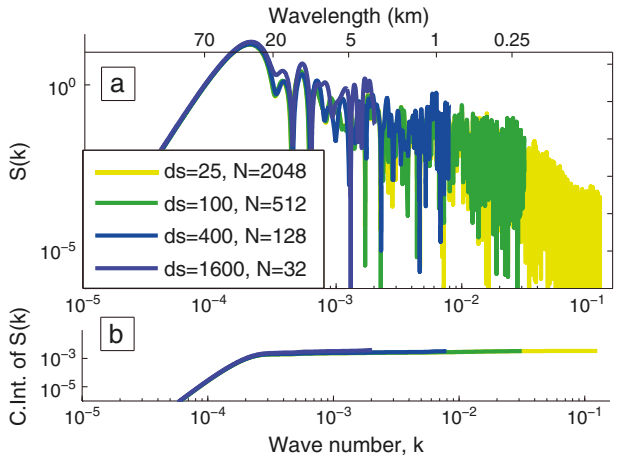

Figure 2. Examples of power spectra for a MW of a fixed length ($L \approx 50$ km), with varying resolutions. (a) Power spectra. (b) Cumulative integral of the power spectra over wave number. *ds* stands for the distance between datapoints in meters and *N* for the number of datapoints.

about the subglacial environment of the former BSIS and the characteristic roughness signature of common subglacial landforms/ice flow regimes, the first steps toward developing a quantitative scheme to characterize subglacial landscapes both contemporary and Quaternary.

2. The Barents Sea

[7] The Barents Sea (BS, Figure 1) covers one of the widest continental shelves in the world. It is bounded to the north and west by tertiary rift and shear margins, to the east by the island of Novaya Zemlya, and to the south by the Norwegian and Russian coasts. Close to the northern boundary are the islands of Svalbard and Franz Josef Land and to the east is the Kara Sea. The sea floor bathymetry is characterized by relatively shallow banks of between 100 and 200 m water depths separated by troughs, opening toward the Norwegian Sea and the Arctic Ocean, of water depths between 300 and 500 m. The most prominent trough is the Bjørnøyrenna (Bear Island Trough), formerly occupied by a major ice stream [*Andreassen and Winsborrow*, 2009]. Separating sedimentary rocks from the overlying Quaternary sediment sequence is the upper regional unconformity representing the most significant seismic reflector in the Barents Sea. On the shelf, the sediment thickness ranges from 0 to around 300 m. Postglacial infilling is limited, with only a thin veneer of Holocene sediments, typically less than 2 m [*Elverhøi and Solheim*, 1983; *Vorren et al.*, 1988]. In some areas, such as on Spitsbergenbanken, the glacial sediments have been reworked by currents and mixed with Holocene bioclastics [*Elverhøi and Solheim*, 1983].

[8] The former BSIS offers a good geological analog to the contemporary WAIS. Similarities between the two ice sheets include a bed largely below sea level resting on sedimentary bedrock, a high-latitude position, and similar sizes during the Last Glacial Maximum (LGM) when both ice sheets were located at or near the shelf break [*Svendsen et al.*, 2004a; *Anderson et al.*, 2002; *Evans et al.*, 2006]. The WAIS grounding line has in some areas retreated up to 1000 km since the LGM, whereas the BSIS went through stepwise retreat with the Barents Sea largely deglaciated by 12 ka BP [*Andreassen et al.*, 2008; *Andreassen and Winsborrow*, 2009; *Winsborrow et al.*, 2010]. A series of grounding-zone wedges and streamlined bed forms can be followed up the Bjørnøyrenna, documenting the retreat of the Bjørnøyrenna Ice Stream (Figure 1).

3. Method

3.1. Roughness Calculations

[9] Roughness is, in general, defined as a relative measure of the degree of irregularity in a surface. The methodology used in this paper follows *Taylor et al.* [2004] and uses a fast Fourier transform (FFT) to convert bed elevations into wavelength spectra. The procedure is applicable, in principle, to any geophysical track line data, as long as the data are of sufficient quality. The FFT requires a fixed spatial sampling interval. Most geophysical data sets have a fixed sampling interval with respect to time so the data have to be interpolated to accommodate that requirement. Any gaps were filled by means of linear interpolation, provided that they were not too long to render that part of the profile unusable. Here we have used a maximum gap length of 7 datapoints (175 m). If any gap was longer than that, the profile was split into separate segments. For each point estimation of roughness, an elevation profile $Z(x)$ of a certain given length l, typically referred to as a moving window (MW), is used. Before passing it through the FFT, it is linearly detrended by subtracting from the raw data a best fit line $Z_{bf}(x)$ through the data itself. This procedure gives a detrended elevation profile $Z_0(x)$ where

$$Z_0(x) = Z(x) - Z_{bf}(x) \quad (1)$$

[10] This decreases the dominance of the very long wavelengths while the small-scale roughness remains largely

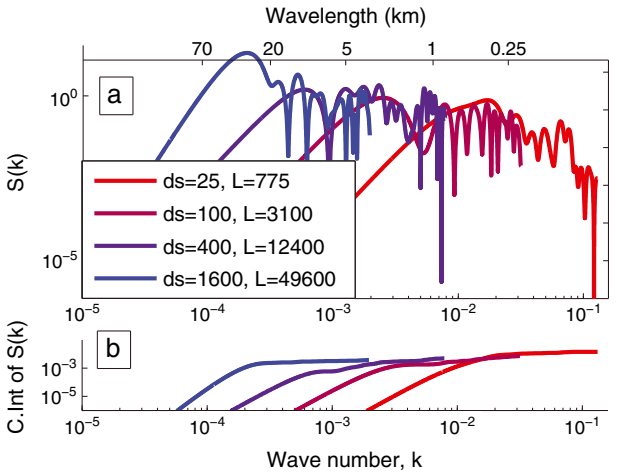

Figure 3. Examples of power spectra for a MW with a fixed number of datapoints ($N = 32$), while varying the distance between them (*ds* [m]). (a) Power spectra. (b) Cumulative integral of the power spectra over wave number. *L* represents the length of the MW in meters.

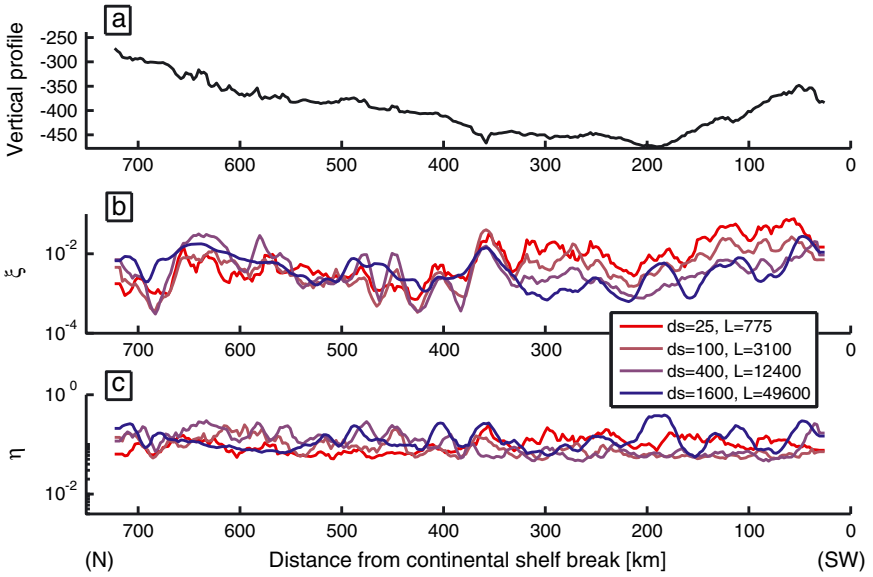

Figure 4. Roughness indices for a track line running from the south of Kong Karls Land to the SW Barents Sea continental shelf break, calculated with a fixed number of datapoints for each point estimate but varying lengths of the MW (L [m]). (a) Elevation profile in meters below sea level. (b) Basal roughness index. (c) η parameter. The horizontal axis in all subfigures shows the distance in kilometers from the continental shelf break.

unaffected [*Shepard et al.*, 2001]. *Li et al.* [2010] introduced a two-parameter index to describe roughness using the slope, $sl(x) = \partial Z_0/\partial x$, of the detrended elevation profile. They showed that although calculating roughness based on the FFT of elevation profiles was a useful way of describing roughness, it might not be sufficient as it only accounts for vertical irregularities in a surface while missing the horizontal ones. They proposed using the slope profile as a link between the horizontal and the vertical undulations. The FFT is calculated for both the detrended elevation and the slope profile, using a minimum of $N = 32$ data points for each MW, and the resulting amplitudes are normalized with $N/2$. The basal roughness index ξ is then defined as the integral of the spectral power density $S(k)$ over the wave numbers k, where $k_1 \rightarrow k_2$ is the range of wave numbers over which the integration is carried, scaled with the length of the MW (equations (2) and (3)). The second roughness parameter η is defined as the ratio of the basal roughness index and the corresponding index ξ_{sl}, calculated with the slope profile (equation (4)).

$$S(k) = \frac{1}{l}|\bar{Z_0}(k)|^2 \tag{2}$$

$$\xi = \int_{k^1}^{k^2} S(k)\mathrm{d}k \tag{3}$$

$$\eta = \frac{\xi}{\xi_{sl}} = \frac{\int_{k_1}^{k_2} S(k)\mathrm{d}k}{\int_{k_1}^{k_2} S_{sl}(k)\mathrm{d}k} = \frac{\int_{k_1}^{k_2} \frac{1}{l}|\bar{Z_0}(k)|^2\mathrm{d}k}{\int_{k_1}^{k_2} \frac{l}{N}|\partial\bar{Z_0}/\partial x|^2\mathrm{d}k} \tag{4}$$

where $\bar{Z_0}(k)$ is the Fourier transform of a detrended elevation profile of a given length l, $\partial\bar{Z_0}/\partial x$ is the Fourier transform for the corresponding slope profile, and $S_{sl}(k)$ is the spectral power density for the slope profile.

[11] The basal roughness index ξ reflects the vertical amplitudes of the profile, so the closer the values are to 0, the smaller the amplitudes and the smoother the bed. The η index represents the horizontal variation with a high value corresponding to a relative dominance of the longer wavelengths while a small value indicates a relative dominance of shorter wavelengths.

3.2. Data and Experiments

[12] Two different sets of data have been used. The first comprises high-resolution (12 m) uninterpolated multibeam bathymetry data collected by the University of Tromsø, and the second is a composite data set of the southwestern Barents Sea. The high-resolution data cover only selected areas including a track line of around 750 km running from the south of Kong Karls Land to the southwestern Bjørnøyrenna continental shelf break (Figure 1). This data set was gridded with a 25 m grid size and a single track line extracted from there. Any gaps in the track line shorter than or equal to 7 times the grid size were filled by linear interpolation. Around 1% of the datapoints from the high-resolution track line were involved in interpolation, and 85% of this was performed over gap lengths of three datapoints or less.

[13] Two kinds of experiments were performed with the track line data. In the first the MW length was kept more or less constant while the number of datapoints varied between comparisons. The absolute length of each MW changes slightly with the number of datapoints ($L = ds(N-1)$) but not to such a degree as to affect the comparison in a significant way. The number of datapoints in each MW ranges from the minimum recommended value of $2^5 = 32$ [*Brigham*, 1988] up to $2^{11} = 2048$ points, making use of the full resolution of our data set for a profile length of 50 km. The length of the MW in the comparison thus varies with maximum 3% between the longest and the shortest one. In the other kind of experiment that was performed, the number of datapoints for each MW was kept constant at $N = 32$ while the distance between the points was progressively doubled

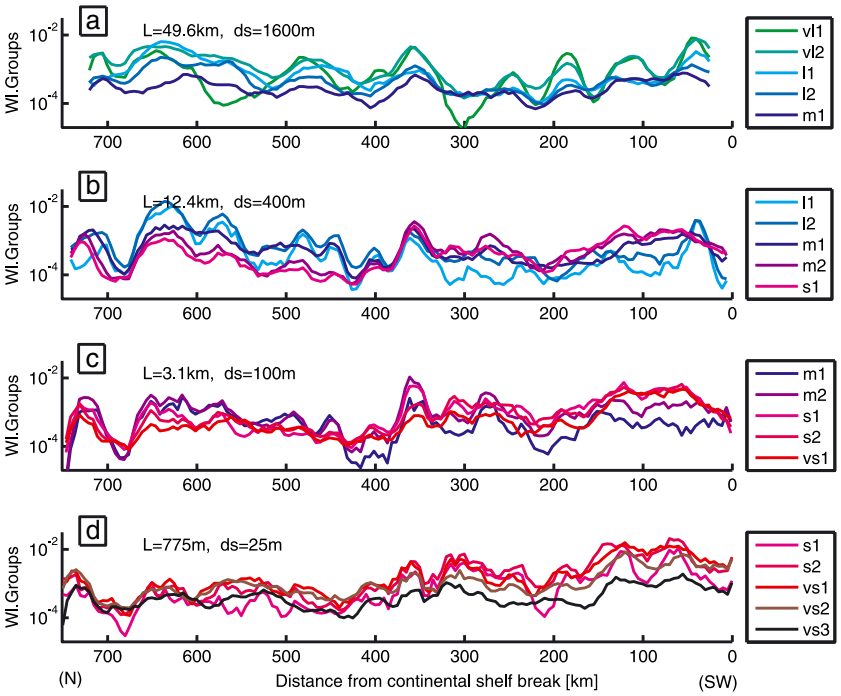

Figure 5. Wavelength components of the four basal roughness profiles (ξ) presented in Figure 4b and with wavelength groups defined by Table 1. Splitting the interval of integration into several subintervals and integrating over them separately reveal which length scales are contributing the most to the basal roughness index (ξ). (a) L = 49.6 km, ds = 1600 m, (b) L = 12.4 km, ds = 400 m, (c) L = 3.1 km, ds = 100 m, and (d) L = 775 m, ds = 25 m.

with each calculation. The MW length thus varied from the shortest possible one of 775 m to the longest one of 49.6 km.

[14] All figures featuring results from these track line data have a horizontal axis indicating distance in kilometers from the continental shelf break and have been smoothed with a five-point moving average to improve readability. These data have been used previously to identify geomorphological features on the seafloor, such as mega-scale glacial lineations (MSGLs) and sedimentary wedges, giving information about past flow directions and grounding line positions [*Rüther et al.*, 2011].

[15] The other data set that was used for this study was a composite data set, created from a dense grid of industry 2-D multichannel seismic data mainly covering the southwestern Barents Sea, single-beam bathymetric data (provided by the Norwegian Defense Research Establishment), and the International Bathymetric Chart of the Arctic Ocean [*Jakobsson et al.*, 2008]. These data sets were merged to give a single bathymetric grid for the entire Barents Sea with a combined horizontal resolution of 600 m. For the purposes of this study, we decided to limit the study area to the southwestern part of the Barents Sea where data coverage and accuracy are highest.

[16] Previous analyses indicate that subglacial roughness is generally an order of magnitude smaller parallel to ice flow direction as compared to the flow-perpendicular direction [*Hubbard et al.*, 2000; *Boulton*, 1979], demonstrating clearly that there is information contained in roughness signatures that can be used to reconstruct former flow directions for deglaciated areas. The composite grid was therefore used to estimate the basal roughness and the directions for which a minimum in roughness was acquired, for the area covering the southwestern Barents Sea.

[17] Profiles of 32 datapoints were extracted from the composite grid using a profile resolution of 1600 m, giving a final length of ~50 km. This resolution was chosen to make the resulting roughness map comparable to similar maps, already published, for various areas in Antarctica [*Siegert et al.*, 2004; *Bingham et al.*, 2007; *Bingham and Siegert*, 2007, 2009; *Rippin et al.*, 2011] and also to minimize the influence of any iceberg ploughmarks in the area, as they then fall beneath or close to the Nyquist frequency and are therefore at the limit of detection. The profiles were extracted over a range of ± 90° from a given reference angle and then used to investigate the orientation dependence of the spectral roughness estimate. The magnitude of orientation dependence (MOD) was quantified in two different

Table 1. Definition of Roughness Wavelengths Used in This Paper, Following *Taylor et al.* [2004]

Wavelength Class	Roughness Wavelength
vl1	>40 km
vl2	20 km–40 km
l1	10 km–20 km
l2	5 km–10 km
m1	2.5 km–5 km
m2	1250 m–2500 m
s1	600 m–1250 m
s2	300 m–600 m
vs1	150 m–300 m
vs2	75 m–150 m
vs3	<75 m

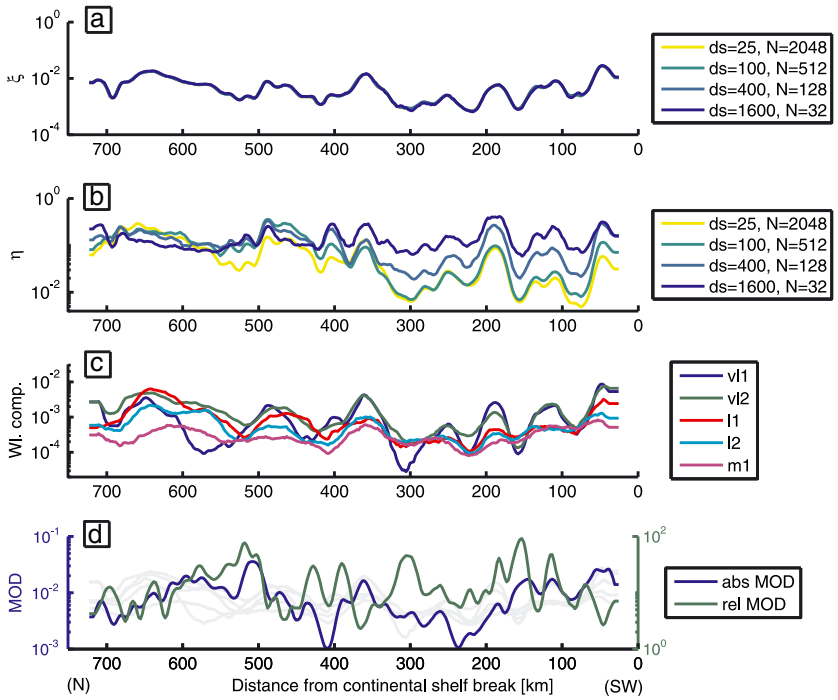

Figure 6. Roughness indices for a track line running from the south of Kong Karls Land to the continental shelf break, calculated with a fixed length of the MW ($L \approx 50$ km), varying the number of datapoints (N) for each estimate. (a) Basal roughness index. Resolution makes little to no difference to the basal roughness index of the profiles. (b) η parameter. (c) Wavelength components for the profile with $ds = 1600$ m and $N = 32$ (blue line). (d) The logarithm of the magnitude of orientation dependence (MOD). The blue line represents the absolute difference between the maximum and the minimum roughness at one point while the green line represents the relative difference (the absolute difference scaled with the minimum value at each point).

ways. First, as the absolute difference between the maximum and the minimum ξ roughness (abs MOD) and second as the logarithm of the ratio between the maximum and the minimum ξ roughness for a single point in space along the track line (rel MOD), depending on orientation. This was done for a network of locations with a fixed spacing of 5 km. All presented results calculated with the composite grid have been averaged over an area of 50×50 km^2 for clarity. The averaged minima directions then served as a basis for the final calculation of the subglacial roughness of the southwestern Barents Sea.

4. Results

4.1. Effect of MW Length and Resolution

[18] The high-resolution data were used to test how the limits of integration (equation (3)) affect the roughness estimate. Figures 2 and 3 show examples of different power spectra for a single location, chosen at random from within the high-resolution bathymetry box in Figure 1 and calculated with either different lengths of the MW and a fixed number of datapoints or by using a different number of datapoints and a fixed length of the MW. The lower part of each figure shows the cumulative integral of each case. In Figure 2, the length of the MW was kept constant at ~50 km, while the number (N) and distance between datapoints (ds) was varied. For each profile, the estimated

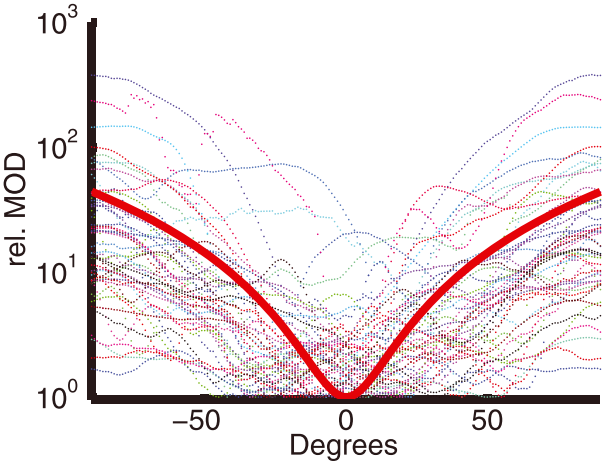

Figure 7. The ξ roughness profiles as a function of orientation. All profiles have been calculated with $N = 32$ and $ds = 1600$ m and then normalized with the minimum roughness values for each respective profile. The profiles were calculated from points representing the whole study area with a regular grid spacing of 100 km. A parabola was fitted to each single profile and then all the profiles were collapsed around their parabolic minima and plotted together. The red thick line represents a parabolic fit to all the data.

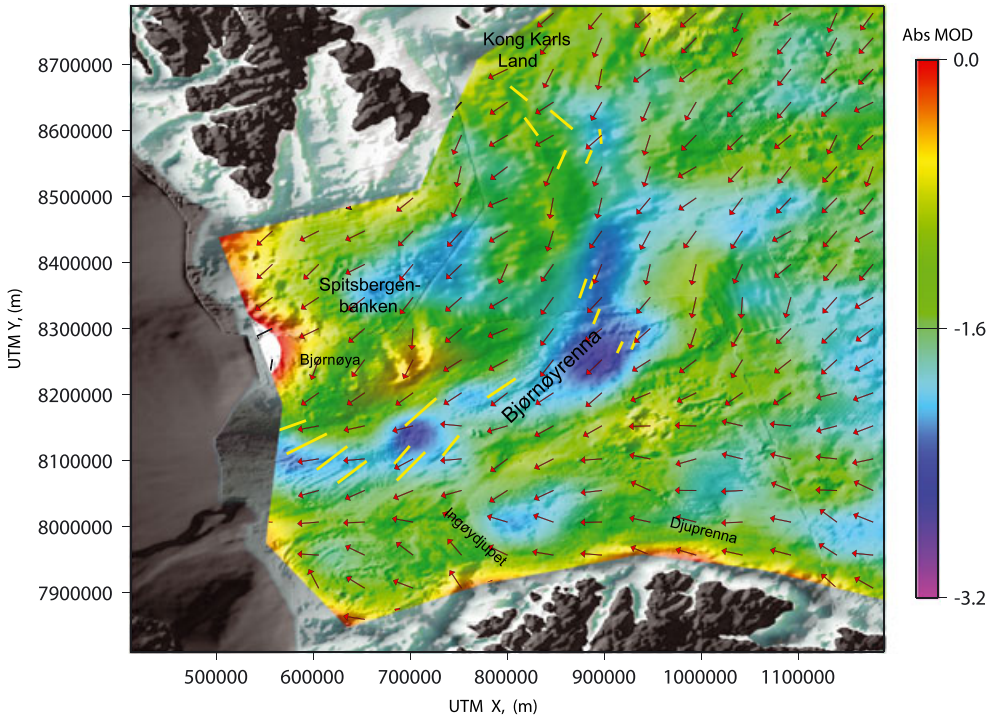

Figure 8. Map showing the spatial variation of the difference between the maximum and the minimum ξ roughness (absolute MOD) depending on orientation. The colorscale shows the logarithmic power of the absolute MOD. Arrows indicate the direction of the roughness minima, and the yellow lines indicate the MSGLs from Figure 1. Both the absolute MOD and the directions of roughness minima have been averaged over an area of $50 \times 50\,\mathrm{km}^2$.

roughness changes only slightly with the number of datapoints used as can be seen from the cumulative integral. That is, resolving the higher frequencies better by simply adding datapoints does not result in a significant change to the roughness estimate.

[19] Figure 3a displays the resulting power spectrum for a fixed number of datapoints, $N = 32$, while the size of the MW decreases from ~50 km to the smallest possible MW (775 m) that our data set allowed, using the full resolution of the data set. Decreasing the MW size while keeping N fixed effectively increases both the lower and the upper wave number limits of integration resulting in a different wave number spectrum for each calculation. In general, for a given location the roughness will vary depending on the size of the MW because of changes in the integration interval as well as changes in the scaling since for each MW the roughness is scaled with the length of that MW.

[20] To further investigate the effect of the MW size and how the resolution of the data affects the roughness estimates, we used a high-resolution track line running from the south of Kong Karls Land to the southwestern Bjørnøyrenna continental shelf break (Figure 1). Figure 4a displays the bathymetry profile in meters below sea level along the 750 km long track line, while Figure 4b shows the spectral roughness for different lengths of the MW. In general, the four different roughness profiles presented here have a similar range of roughness values. However, the roughness is noticeably higher as the size of the MW decreases for the downstream half of the track line. Figure 4c shows the η index, which accounts for horizontal irregularities. With the scaling that was introduced (equation (4)), the η profiles all show a similar range of values, with values roughly above 10^{-1} having a stronger relative dominance of longer wavelengths.

[21] Figure 5 reveals the wavelength components, as defined by Table 1, of the four roughness profiles presented in Figure 4b. Splitting the integration (equation (3)) over different intervals reveals which wavelength components contribute the most to the ξ roughness index. The sum of the different components for each MW length equals the total value seen in Figure 4b. A relative dominance of longer wavelengths corresponds with a peak in the η index (Figure 5). The wavelength group s1, which corresponds to 600–1250 m, is particularly dominant in the downstream half of the trough which is probably due to an increased density of iceberg ploughmarks in the area.

[22] In Figure 6a, we present four different roughness profiles from Bjørnøyrenna, all calculated with the same length of the MW but using a different number of datapoints for each estimate. The differences between the four different profiles are minimal, which can be seen as verification for the fact that 32 datapoints for each profile are adequate for roughness calculations of this type. Figure 6b shows the four different η profiles. With increasing resolution, the slope profile (equation (4)) gets progressively rougher for the lower half of the track line, resulting in lower η values. Figure 6c shows the individual contributions from the different wavelength components of roughness (Table 1) for the profile with the largest distance between datapoints (ds = 1600 m).

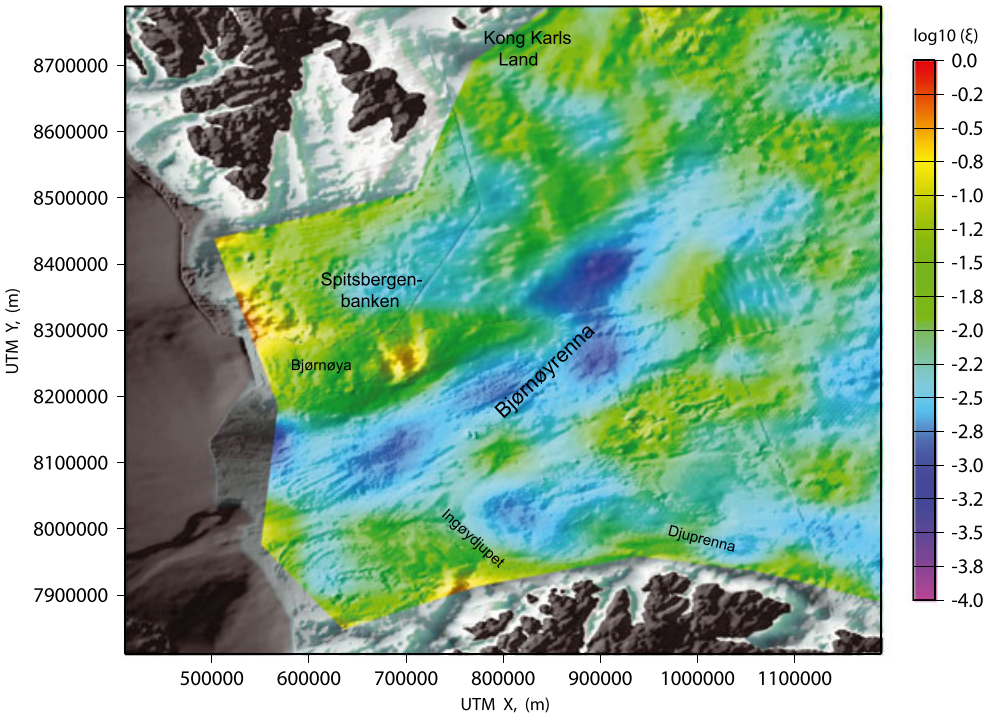

Figure 9. Map of basal roughness (ξ) for the western Barents Sea. The colorscale represents the logarithmic power of the basal roughness index. This is calculated using 32 datapoints (N) for each point estimation and with a distance of 1600 m between each datapoint (ds).

4.2. MW Orientation and Angle Dependence

[23] The blue and the green lines in Figure 6d represent the absolute MOD and the relative MOD, respectively. The absolute MOD shows a moderate correlation with ξ roughness, while the relative MOD shows a moderate anticorrelation. In both cases the correlation grows stronger with increasing wavelength.

[24] For glaciated terrains like Antarctica or Greenland, roughness estimates are usually queried along flight tracks of preimposed orientation and not necessarily in the direction of ice flow. This entails some deviation from the roughness that the ice actually experiences as the roughness is generally expected to have a minimum in the flow direction.

[25] The variation of ξ roughness with orientation is presented in Figure 7 for a number of locations in the southwestern Barents Sea. The locations were chosen by overlaying a fixed 100 km × 100 km grid over the region and performing the calculation at each equally spaced vertex. The locations are therefore representative of the entire study area. A parabolic curve was fitted to each individual profile because of its simple representation and single minimum, and then all profiles were plotted together, ranging from –90° to +90°, with their parabolic minimum at the center. The thick red line in Figure 7 represents a best fit through all the profiles with linear regression. The roughness estimate shows a strong dependence with direction and typically a 40-fold difference between the minimum roughness value at one point and the maximum. The variation is, however, quite large and maximum values range from a few times the minimum to around 400 times the minimum. A strong angle dependence is shown for all wavelength groups, but the minimum is not always acquired at the same angle within each group, although the variation between each group is usually small.

[26] Furthermore, the calculation with the 5 km spacing was used in order to examine the spatial distribution of the absolute MOD, which is presented in Figure 8.

[27] By averaging the angles at which a minimum in roughness was acquired, we end up with a directional map that should resemble a map of former ice flow directions for the western Barents Sea at the time of the last glaciation. The arrows in Figure 8 indicate the averaged directions of the roughness minima. These directions were then used as a basis for the roughness map shown in Figure 9.

5. Discussion

5.1. Geomorphic Features

[28] Our results show opposing trends between the large-scale and the small-scale roughness. The large-scale roughness typically decreases until the deepest point of Bjørnøyrenna, while the small-scale roughness shows more or less a continuous increase in measured roughness toward the continental shelf break (Figure 4). We interpret this as being caused mostly by the increasing density of iceberg ploughmarks toward the shelf break. Close to the shelf break, an area of around 3000 km^2 in size (Figure 1; yellow box) has been mapped for geomorphological purposes [*Rüther et al.*, 2011], and that part of the trough has a very dense network of iceberg ploughmarks. Iceberg ploughmarks have a typical length scale of between tens of meters up to several hundred meters across the ploughmark and will therefore cause an increase in measured roughness over

these length scales. These ploughmarks also introduce sharp bathymetry gradients which become clearer and sharper with higher resolution. These cause a decrease in the η parameter with increasing resolution because of the increased relative importance of the shorter wavelengths (Figure 6).

[29] Several ice-marginal deposits have been identified in the area (Figure 1) [*Winsborrow et al.*, 2010], and these are typically represented by a sharp peak in roughness, especially at longer wavelengths and by a local increase in absolute MOD (Figures 5 and 6). Figure 4 illustrates how the different roughness profiles diverge away from one another roughly 375 km away from the shelf break at a point which corresponds to a local minimum in elevation. Close to this point, an ice-marginal deposit has been mapped which may have been a stable grounding line position for some time during the deglaciation period. Downstream of that location, the small-scale roughness increases, especially in the "s1" wavelength group, while the longer wavelengths stay at a more or less constant low level.

[30] Three peaks in roughness are observed in Figure 5b between the 500 km and the 400 km marks that correspond to geomorphic features that have been mapped as possible ice margins (Figure 1). These have a characteristic signal of increased long wavelength roughness, and their locations can be picked out easily from roughness diagrams. Where a multibeam track line comprises the only available data, such roughness analysis might therefore give valuable information as to the whereabouts of ice-marginal deposits and possibly other geomorphic features that the track line crosses. However, more data and further analyses are necessary for verification. Both ploughmarks and ice-marginal deposits cause a change in measured roughness as compared to the roughness of the ice sheet bed at the time of the LGM. No detailed map of Holocene sediments is available for the Barents Sea, but sedimentation rates for the southwestern Barents Sea are in general thought to be quite low. A thin drape (< 2 m) of Holocene sediments covers most of the Barents Sea [*Elverhøi and Solheim*, 1983] which will primarily affect roughness measurements on very small scales. Here we look at roughness on the scale of several kilometers down to tens of meters; hence, postglacial modification caused by ocean currents and marine sedimentation is therefore not considered to be an issue of significant importance.

5.2. Effect of MW Length and Resolution

[31] As noted earlier, an important question concerning subglacial roughness captured along RES tracks is how the roughness estimate is affected by the sampling resolution of the tracks and the length of the MW. Our results indicate that the roughness estimate is strongly dependent on the length of the MW but not so much on the sampling resolution, provided that an adequate number of datapoints has been used for each point estimation. Increasing the number of datapoints for each roughness estimation, and thereby increasing the upper wave number limit for integration, does not lead to a significantly different roughness estimate for a fixed length of the MW (Figures 2, 3, and 6). In our case, however, it does result in a lower η index as the slope profile appears rougher with increasing resolution. The ξ roughness index remains unchanged, but the effect is seen clearly on the power spectrum of the slope profile (ξ_{sl}), causing it to become greater such that consequently the ratio (η) between the two drops. This is not representative for a presently glaciated area though, as a large part of the change is due to the presence of iceberg ploughmarks. On the other hand, this shows that roughness analysis of this type can be a valuable tool in the interpretation of subglacial landforms.

[32] The η parameter proves to be a very convenient way of continuously expressing the horizontal irregularities, although similar information can be acquired by looking at the different contributions from the different wavelength groups. In general, an increase in the η index results from an increased relative importance of the longer wavelengths, as can be seen from Figures 4, 5, and 6. Here the η index is small where the small-scale roughness is dominant and large when large-scale roughness is dominant.

5.3. Orientation Dependence

[33] Bed elevation and ice thickness data are acquired along flight tracks, usually in straight lines and not necessarily in the direction of ice flow. Although it is tempting to use all bed elevation data for roughness studies, our results show that changing the orientation of a single elevation profile extracted for roughness measurements can significantly change the calculated spectral roughness for that point in space. The relative difference between the minimum and the maximum roughness depending on orientation can be up to several orders of magnitude (Figure 7). This angle dependence is observed for all wavelength groups, as well as for the η index, indicating increased dominance of longer wavelengths in the across flow direction as compared to along flow. Curves showing roughness as a function of orientation can also have multiple minima, possibly related to changes in ice flow direction in the past. For deglaciated areas like the Barents Sea, many geomorphological features reveal the direction of former ice flow, like mega-scale glacial lineations (MSGLs) and drumlins. These can be compared to the orientations for which a minimum in roughness is acquired. In Figure 8, several MSGLs are presented that have been mapped and associated with various retreat stages of the BSIS [*Winsborrow et al.*, 2010]. Each retreat stage can be associated with a different time period and a different ice sheet configuration and thus possibly with somewhat different ice flow directions for each stage. The apparent mismatch between the directions of roughness minima and the MSGLs is thought to stem from the fact that roughness on this spatial scale is likely to reflect the integrated effect of erosion and deposition over longer time scales, whereas the MSGLs can only be related to flow directions at the time of formation. Part of the high-resolution data used for this study also contained several MSGLs (Figure 1; red lines, yellow box), the orientation of which had a direction that differed only by 2° from the estimated past flow direction based on roughness analysis. In this case the MW was chosen to be as large as the high-resolution databox allowed (20 km) in order to minimize the effect of the MSGLs on the spectral roughness. A smaller MW with this data set would have resulted in an even stronger contrast between a flow-parallel and a flow-perpendicular direction so that even over larger spatial scales, the bed in the flow direction is preferentially smoothed past a threshold sufficient for it to become measurable by the spectral roughness method. Our data also show a moderate correlation between the strength of the absolute orientation dependence (abs. MOD) and the

ξ roughness parameter as well as a moderate anticorrelation between the relative MOD and ξ, with the correlation growing stronger with increasing wavelength (Figures 6, 8, and 9).

5.4. Geographical Distribution of Roughness

[34] In general, for long MW, the roughness is smaller in Bjørnøyrenna than in adjacent areas (Figure 9) as expected for an area of fast flow and high rates of basal erosion [*Bingham and Siegert*, 2007]. A zone of low roughness is also seen in Djuprenna while Ingøydjupet has considerably higher roughness compared with the other troughs in the study area. In both of these locations, ice streams also operated (Figure 1). Spitsbergenbanken shows the highest roughness values of the whole study area. This is a submarine bank area, with typical water depths of between 40 m and 60 m, and it is one of the shallowest areas of the Barents Sea. It has experienced very little glacial erosion in the last 0.7 Ma compared with the troughs [*Laberg et al.*, 2011], and ice flow over it is likely to have been considerably slower.

[35] Similar roughness calculations have been completed for various, previously marine-inundated areas in Antarctica using RES data and MWs of between 1 km and 100 km. The roughness values that we get for the southwestern Barents Sea range from 10^{-4} to 10^{-1} for all lengths of the MW, consistent with those found beneath both Pine Island Glacier (PIG) [*Rippin et al.*, 2011] and in the Siple Coast region [*Siegert et al.*, 2004], where the low roughness values have been considered as a first-order indicator of a previous marine inundation and sediment drape [*Bingham and Siegert*, 2009]. The southwestern Barents Sea shows somewhat higher roughness values than the PIG catchment even though the roughness values from the PIG area have not always been calculated in the flow direction and also with a different length of the MW. These three geographically distinct areas, all previously marine inundated in the past, share a similar roughness signature.

6. Conclusions

[36] Using bathymetry data from shipborne 2-D and 3-D seismics and multibeam sonar, the subglacial roughness of a Quaternary glaciated terrain has, for the first time, been quantified. This yields roughness estimates of higher resolution, greater coverage, and at a wider range of scales, than are possible with most existing Antarctic radio echo sounding data sets. The roughness index varies insignificantly with resolution for a fixed length of the moving window (MW) and with constant scaling, but both roughness parameters show considerably more variation as the length of the MW changes. This implies that roughness measurements from different studies are not directly comparable unless calculated with similar lengths of the MW. A strong dependence on orientation is observed for both roughness parameters, as well as for all wavelength groups. Even a small deviation, on the order of a few degrees, can cause a significant change in estimated roughness, and care must be taken when interpreting such roughness estimates for track lines that are not in the flow direction. Rougher areas typically have a stronger absolute orientation dependence and a weaker relative one.

[37] Here we have provided the first confirmation that a Quaternary glaciated region of the world that has also experienced several cycles of glaciations in the past interspersed with interglacial marine inundations [*Svendsen et al.*, 2004a], much like the Siple Coast region or Pine Island Glacier, has imprinted a similar roughness signature [*Bingham and Siegert*, 2009; *Rippin et al.*, 2011]. This provides promise that as more roughness analysis on glacially defined surfaces emerges, it may be possible to develop a quantitative scheme to characterize subglacial landscapes in the future.

[38] **Acknowledgments.** Funding for this work came from the Research Council of Norway (RCN), Statoil, Det Norske ASA, and BG group Norway (grant 200672) to the PetroMaks project Glaciations in the Barents Sea area (GlaciBar) and from the Research School in Arctic Marine Geology and Geophysics (AMGG) at the University of Tromsø. This is also a contribution to the Centre of Excellence: Arctic Gas Hydrate, Environment and Climate (CAGE) funded by RCN (grant 223259). We thank the captain and crew of R/V Helmer Hanssen (previously Jan Mayen), and Steinar Iversen for collecting and processing of the data. We would also like to thank R.G. Bingham, the associate editor M.J. Bentley, and one anonymous reviewer for their constructive reviews that greatly improved the manuscript.

References

Anderson, J. B., S. S. Shipp, A. L. Lowe, J. S. Wellner, and A. B. Mosola (2002), The Antarctic Ice Sheet during the Last Glacial Maximum and its subsequent retreat history: A review, *Quat. Sci. Rev.*, *21*(1), 49–70.

Andreassen, K., and M. Winsborrow (2009), Signature of ice streaming in Bjørnøyrenna, Polar North Atlantic, through the Pleistocene and implications for ice-stream dynamics, *Ann. Glaciol.*, *50*(52), 17–26.

Andreassen, K., J. S. Laberg, and T. O. Vorren (2008), Seafloor geomorphology of the SW Barents Sea and its glaci-dynamic implications, *Geomorphology*, *97*(1-2), 157–177.

Bingham, R. G., and M. J. Siegert (2007), Radar-derived bed roughness characterization of Institute and Möller ice streams, West Antarctica, and comparison with Siple Coast ice streams, *Geophys. Res. Lett.*, *34*, L21504, doi:10.1029/2007GL031483.

Bingham, R. G., and M. J. Siegert (2009), Quantifying subglacial bed roughness in Antarctica: Implications for ice-sheet dynamics and history, *Quat. Sci. Rev.*, *28*(3-4), 223–236.

Bingham, R. G., M. J. Siegert, D. A. Young, and D. D. Blankenship (2007), Organized flow from the South Pole to the Filchner-Ronne ice shelf: An assessment of balance velocities in interior East Antarctica using radio echo sounding data, *J. Geophys. Res.*, *112*, F03S26, doi:10.1029/2006JF000556.

Boulton, G. S. (1979), Processes of glacier erosion on different substrata, *J. Glaciol.*, *23*(89), 15–38.

Brigham, E. O. (1988), The fast Fourier transform and its applications, *IEEE Trans. Educ.*, *12*(1), 27–34.

Elverhøi, A., and A. Solheim (1983), The Barents Sea ice sheet: A sedimentological discussion, *Polar Res.*, *1*(1), 23–42.

Evans, J., J. A. Dowdeswell, C. Ó Cofaigh, T. J. Benham, and J. B. Anderson (2006), Extent and dynamics of the West Antarctic ice sheet on the outer continental shelf of Pine Island bay during the last glaciation, *Mar. Geol.*, *230*(1), 53–72.

Fowler, A. C. (1979), A mathematical approach to the theory of glacier sliding, *J. Glaciol.*, *23*, 131–141.

Fowler, A. C. (1981), A theoretical treatment of the sliding of glaciers in the absence of cavitation, *Philos. Trans. R. Soc. London, Ser. A*, *298*(1445), 637–681.

Gudmundsson, G. H. (1997a), Basal-flow characteristics of a non-linear flow sliding frictionless over strongly undulating bedrock, *J. Glaciol.*, *43*(143), 80–89.

Gudmundsson, G. H. (1997b), Basal-flow characteristics of a linear flow sliding frictionless over small bedrock undulations, *J. Glaciol.*, *43*(143), 71–79.

Hubbard, B., M. J. Siegert, and D. McCarroll (2000), Spectral roughness of glaciated bedrock geomorphic surfaces: Implications for glacier sliding, *J. Geophys. Res.*, *105*(B9), 21,295–21,303.

Jakobsson, M., R. Macnab, L. Mayer, R. Anderson, M. Edwards, J. Hatzky, H. W. Schenke, and P. Johnson (2008), An improved bathymetric portrayal of the Arctic Ocean: Implications for ocean modeling and geological, geophysical and oceanographic analyses, *Geophys. Res. Lett.*, *35*, L07602, doi:10.1029/2008GL033520.

Kamb, B. (1970), Sliding motion of glaciers: Theory and observation, *Rev. Geophys.*, *8*(4), 673–728.

Laberg, J. S., K. Andreassen, and T. O. Vorren (2011), Late Cenozoic erosion of the high-latitude southwestern Barents Sea shelf revisited, *Geol. Soc. Am. Bull.*, *124*(1-2), 77–88.

Li, X., B. Sun, M. J. Siegert, R. G. Bingham, X. Tang, D. Zhang, X. Cui, and X. Zhang (2010), Characterization of subglacial landscapes by a two-parameter roughness index, *J. Glaciol.*, *56*(199), 831–836.

Nye, J. F. (1970), Glacier sliding without cavitation in a linear viscous approximation, *Proc. R. Soc. London, Ser. A*, *315*(1522), 381–403.

Rippin, D. M., D. G. Vaughan, and H. F. J. Corr (2011), The basal roughness of Pine Island Glacier, West Antarctica, *J. Glaciol.*, *57*(201), 67–76.

Rüther, D. C., R. Mattingsdal, K. Andreassen, M. Forwick, and K. Husum (2011), Seismic architecture and sedimentology of a major grounding zone system deposited by the Bjørnøyrenna Ice Stream during Late Weichselian deglaciation, *Quat. Sci. Rev.*, *30*(19), 2776–2792.

Shepard, M. K., B. Campbell, M. H. Bulmer, T. G. Farr, L. R. Gaddis, and J. J. Plaut (2001), The roughness of natural terrain: A planetary and remote sensing perspective, *J. Geophys. Res.*, *106*, 32,777–32,795.

Siegert, M. J., J. Taylor, A. J. Payne, and B. Hubbard (2004), Macro-scale bed roughness of the Siple Coast ice streams in West Antarctica, *Earth Surf. Processes Landforms*, *29*(13), 1591–1596.

Siegert, M. J., J. Taylor, and A. J. Payne (2005), Spectral roughness of subglacial topography and implications for former ice-sheet dynamics in East Antarctica, *Global Planet. Change*, *45*(1), 249–263.

Svendsen, J. I., V. Gataullin, J. Mangerud, and L. Polyak (2004a), The glacial history of the Barents and Kara Sea region, *Dev. Quat. Sci.*, *2*, 369–378.

Svendsen, J. I., et al. (2004b), Late Quaternary ice sheet history of northern Eurasia, *Quat. Sci. Rev.*, *23*(11), 1229–1271.

Taylor, J., M. J. Siegert, A. J. Payne, and B. Hubbard (2004), Regional-scale bed roughness beneath ice masses: Measurement and analysis, *Comput. Geosci.*, *30*(8), 899–908.

Vorren, T. O., M. Hald, and E. Lebesbye (1988), Late Cenozoic environments in the Barents Sea, *Paleoceanography*, *3*(5), 601–612.

Weertman, J. (1957), On the sliding of glaciers, *J. Glaciol.*, *3*(21), 33–38.

Winsborrow, M., K. Andreassen, G. D. Corner, and J. S. Laberg (2010), Deglaciation of a marine-based ice sheet: Late Weichselian palaeo-ice dynamics and retreat in the southern Barents Sea reconstructed from onshore and offshore glacial geomorphology, *Quat. Sci. Rev.*, *29*(3), 424–442.

Paper 2

Gudlaugsson, E., Humbert, A., Kleiner, T., Kohler, J., and Andreassen, K., (2015), The influence of a model subglacial lake on ice dynamics and internal layering, The Cryosphere Discuss., 9, 3859-3886, doi:10.5194/tcd-9-3859-2015.

UiT / THE ARCTIC UNIVERSITY OF NORWAY

The influence of a model subglacial lake on ice dynamics and internal layering

Eythor Gudlaugsson[1], Angelika Humbert[2,3], Thomas Kleiner[2], Jack Kohler[4], and Karin Andreassen[1]

[1]Centre for Arctic Gas Hydrate, Environment and Climate (CAGE), Department of Geology, UiT – The Arctic University of Norway, Tromsø, Norway
[2]Section of Glaciology, Alfred Wegener Institute Helmholtz Center for Polar and Marine Research, Bremerhaven, Germany
[3]Department of Geosciences, University of Bremen, Bremen, Germany
[4]Norwegian Polar Institute, Fram Centre, Tromsø, Norway

Correspondence to: Eythor Gudlaugsson (eythor.gudlaugsson@uit.no)

Abstract. As ice flows over a subglacial lake, the drop in bed resistance leads to an increase in ice velocities and a subsequent draw-down of isochrones and cold ice from the surface. The ice surface flattens as it adjusts to the lack of resisting forces at the base. The rapid transition in velocity induces changes in temperature and ice viscosity, releasing deformation energy which raises the temperature locally. Recent studies of Antarctic subglacial lakes indicate that many lakes experience very fast and possibly episodic drainage, during which the lake size is rapidly reduced as water flows out. A question is what effect this would have on internal layers within the ice, and whether such past events could be inferred from isochrone structures downstream.

Here, we study the effect of a subglacial lake on the dynamics of a model ice stream as well as the influence that such short timescale drainage would have on the internal layers of the ice. To this end, we use a Full-Stokes, polythermal ice flow model.An enthalpy gradient method is used to account for the evolution of temperature and water content within the ice.

We find that the rapid transition between slow-moving ice outside the lake, and full sliding over the lake, releases large amounts of deformational energy, which has the potential to form a temperate layer at depth in the transition zone. In addition, we provide an explanation for a characteristic surface feature, commonly seen at the edges of subglacial lakes, a hummocky surface depression in the transition zone between little to full sliding. We also conclude that rapid changes in lake geometry or basal friction create a travelling wave at depth within the isochrone structure that transfers downstream with the advection of ice, thus indicating the possibility of detecting past events with ice penetrating radar.

1 Introduction

Nearly 400 subglacial lakes have been identified in Antarctica based on radar data and satellite measurements (Wright and Siegert, 2012), as well as at least two subglacial lakes in Greenland, all of which satisfy established criteria for identification of subglacial lakes (Palmer et al., 2013). Subglacial lakes are typically either located in the ice-sheet interior, close to ice divides where surface slopes are low and ice is thick, or in areas of higher ice velocity where internal ice deformation and sliding add to geothermal energy to produce melting at the base (Siegert et al., 1996; Dowdeswell and Siegert, 1999).

Subglacial lakes have been hypothesized to play a role in the initiation of fast flow by either 1) providing a steady stream of water downstream of their location, lubricating the base (Gray et al., 2005; Langley et al., 2014), 2) substantially influencing the thermal regime of the ice, gradually warming the basal ice from below, or 3) providing ice with enough thermal momentum to resist freezing on downstream of the lake (Bell et al., 2007).

The reason why so few lakes have been discovered in Greenland, despite considerable efforts and relatively dense surveying compared to Antarctica, is believed to be because of the generally warmer ice and higher surface slopes in Greenland, which favour rapid and more efficient drainage as well as increased vulnerability to drainage instabilities (Pattyn, 2008). In addition, the large supply of surface meltwater to the base of the Greenland ice sheet through hydrofracturing means that the drainage networks in place are probably already highly efficient, and thus capable of effectively draining subglacial water and preventing or limiting subglacial lake development (Palmer et al., 2013).

Apart from lake Vostok, the largest subglacial lake in the world as well as a few other ones, the typical subglacial lake is around $10\,\mathrm{km}$ in diameter (Siegert, 2000). Recent studies have presented compelling evidence of rapid transport of water stored in subglacial lakes indicating that lakes can either drain episodically, or transiently on relatively short time scales (Gray et al., 2005; Wingham et al., 2006; Fricker et al., 2007). Lakes appear to form a part of a connected hydrological network, with upstream lakes draining into downstream ones as subglacial water moves down the hydrological potential (Siegert et al., 2007). Both ice and water transport a substantial amount of sediment over time which is deposited in the lakes, thus reducing their size over long time scales. Sedimentation rates can vary from close to zero to several millimetres per year, with sediment layers estimated to be up to several hundreds of meters thick in some lakes (Christoffersen et al., 2008; Bentley et al., 2013). The dominant mechanism in transporting sediment to subglacial lakes is thought to be influx of sediment-laden water for open-system, or active lakes, and melt-out from the overlying ice for closed-system lakes, where water exchange happens purely through melting and freezing (Bentley et al., 2013). Subglacial lakes thus change size on a variety of time scales with different mechanisms, from fast drainage to slow sedimentation.

The presence of a subglacial lake is often signalled by a flattening of the ice surface, given that the lake is in hydrostatic equilibrium and as a local speed-up of ice velocities. This draws down cold ice and deflects isochrone layers within the ice (Weertman, 1976).

Numerous studies have investigated the effect of spatially varying basal (or surface) conditions on ice dynamics and the internal layering of ice, such as melting or basal resistance. Previously, Leysinger-Vieli et al. (2007) studied the effect of a subglacial lake on isochrones by prescribing the flow and then solving for the age of ice. The effect of a subglacial lake on ice dynamics was investigated by Sergienko et al. (2007), who used a 2D vertically-integrated flow equation to study ice sheet response to transient changes in lake geometry and basal resistance, and by Pattyn (2008) who investigated the stability of a subglacial lake to drainage events. The interaction between lake circulation and ice dynamics and its effect on the basal mass balance has also been studied by Thoma et al. (2010).

The aim of this study is to investigate the influence of a subglacial lake on the dynamics of a model ice stream and the effect it has on the isochrone structure within the ice. As all stress components are important for such an interaction, we use a fully 3D thermo-mechanically coupled Full Stokes ice sheet model, implemented in the commercial finite element software COMSOL. We employ an enthalpy-gradient method to account for the softening effect of ice temperature and water content on ice viscosity (Aschwanden et al., 2012) and we show how temporally varying basal conditions can lead to the appearance of flow bands, or arches and troughs, within the internal layering downstream of the original flow disturbance.

2 Model Description

Ice Flow

Ice is treated as an incompressible fluid with constant density, obeying conservation laws for mass and momentum:

$$\boldsymbol{\nabla} \cdot \boldsymbol{u} = 0 \tag{1}$$

and

$$\boldsymbol{\nabla} \cdot \boldsymbol{\sigma} = -\rho \boldsymbol{g}, \tag{2}$$

where $\boldsymbol{u}$ is the velocity vector, $\boldsymbol{g}$ the gravitational acceleration, ρ the ice density and $\boldsymbol{\sigma}$ the Cauchy stress tensor. The Cauchy stress tensor is given by:

$$\boldsymbol{\sigma} = \boldsymbol{\tau} - p\boldsymbol{I}, \tag{3}$$

where $\boldsymbol{\tau}$ and $p\boldsymbol{I}$ are the deviatoric and the isotropic parts, p is pressure, and $\boldsymbol{I}$ is the identity matrix. Inertial forces are assumed negligible and only body forces arising from gravity are taken into account.

Ice is assumed to follow Glen's flow law (Steinemann, 1954; Glen, 1955), in which deviatoric stresses are related to strain rates ($\dot{\boldsymbol{\varepsilon}}$) by:

$$\boldsymbol{\tau} = 2\eta\dot{\boldsymbol{\varepsilon}} \tag{4}$$

and

$$\eta(T^{'},\dot{\varepsilon_e}) = \frac{1}{2}[A_t(T^{'},W)]^{-\frac{1}{n}}\dot{\varepsilon_e}^{\frac{1-n}{n}}, \tag{5}$$

where η is the effective viscosity, $\dot{\varepsilon_e}$ is the effective strain rate, $T^{'} = T + \gamma p$ is the homologous temperature which corrects for the dependence of the pressure-melting point (T_m) on pressure, γ is the Clausius-Clapeyron constant, and n is the power-law exponent in Glen's flow law. The rate factor (A_t) depends on temperature (T), pressure and the water content (W) of the ice as follows (Duval, 1977):

$$A_t(T,p,W) = A(T,p) \times (1 + 1.8125W[\%]), \tag{6}$$

where

$$A(T,p) = A(T^{'}) = A_0 e^{-Q/RT^{'}}, \tag{7}$$

and A_0 is a pre-exponential constant, Q is the activation energy and R is the universal gas constant (Greve and Blatter, 2009).

Enthalpy balance

An enthalpy-gradient method (Aschwanden et al., 2012) is employed, as opposed to the typically used cold-ice formulation, which is incapable of correctly reproducing the rheology of temperate layers within ice sheets. The enthalpy formulation allows for the possibility of including liquid water content within temperate ice, based on mixture theory, without explicitly tracking the cold/temperate transition surface (Aschwanden et al., 2012; Greve, 1997). In the enthalpy-gradient method, enthalpy replaces temperature as the thermodynamical state variable, such that:

$$\rho\left(\frac{\partial H}{\partial t} + \boldsymbol{u}\cdot\nabla H\right) = \boldsymbol{\nabla}\cdot\left(\left\{\begin{array}{c} K_i(H)\nabla H \\ k(H,p)\nabla T_m(p) + K_0\nabla H \end{array}\right\}\right) + Q, \tag{8}$$

where $H = H(T,W,p)$ is the temperature and water content dependent specific enthalpy, T_m the pressure melting point, and $Q = 4\eta\dot{\varepsilon_e}^{\,2}$ is the heat dissipation due to internal deformation. The conduction term in Eq. (8) depends on whether the ice is cold ($H < H_{T_m}(p)$) or temperate ($H \geq H_{T_m}(p)$). The conduction coefficient for cold is ice defined as $K_i = k/c$, where k is the thermal conductivity and c is the heat capacity, both assumed to be constant. $H_{T_m}(p)$ is the specific enthalpy of the pressure dependent melting point of ice. The diffusivity for temperate ice is poorly constrained as little is known about the transport of microscopic water within temperate ice (Aschwanden et al.,

2012; Hutter, 1982). In practice, we use the value $K_0 = 10^{-3}K_i$, shown by Kleiner et al. (2015) to be sufficiently low to suppress transport of water by diffusion through the ice matrix, while still numerically stable.

Age equation

In addition to the balance equations above, we solve a separate equation for the ice age (χ) to determine the influence of the lake on the isochrone structure (Hindmarsh et al., 2009; Parrenin et al., 2006; Parrenin and Hindmarsh, 2007; Leysinger-Vieli et al., 2007):

$$\frac{\partial \chi}{\partial t} + \boldsymbol{u} \cdot \nabla \chi = 1 + (d_\chi \nabla^2 \chi), \tag{9}$$

where χ is the age of ice and the second term on the right represents a diffusivity term needed for numerical stability, in which d_χ is the numerical diffusivity.

Boundary conditions

At the surface, stresses arising from atmospheric pressure and wind can be neglected as they are very small compared to the typical stresses in the ice sheet (Greve and Blatter, 2009), resulting in a traction-free boundary condition (BC),

$$\boldsymbol{\sigma} \cdot \boldsymbol{n} = 0, \tag{10}$$

where $\boldsymbol{n}$ is the normal vector pointing away from the ice. Accumulation and ablation (a_s) at the surface are assumed to be zero, giving the kinematic surface BC as:

$$\frac{\partial z_s}{\partial t} + u\frac{\partial z_s}{\partial x} + v\frac{\partial z_s}{\partial y} - w = a_s = 0, \tag{11}$$

where z_s is the surface elevation. We employ an inverse Weertman-type sliding law (Eq. 12), where the basal drag ($\boldsymbol{\tau_b}$) is expressed as a function of the velocity of the ice ($\boldsymbol{u_b}$) immediately above the ice/base interface, except over the lake surface where basal traction is set to zero (full slip). With basal sliding exponents $(p,q) = (1,0)$ appropriate for ice streaming conditions, the sliding relationship simplifies to a linear relationship between basal sliding and basal traction. Ice accretion and melt at the base are assumed to be zero and along with the stress BC at the surface, a no-penetration condition is used to close the system:

$$\boldsymbol{u_b} = -C^{-1}\frac{|\tau_b|^{p-1}\boldsymbol{\tau_b}}{{N_b}^q} = -C^{-1}\boldsymbol{\tau_b} \qquad \Rightarrow \qquad \boldsymbol{\tau_b} = C\boldsymbol{u_b}, \tag{12}$$

and

$$\boldsymbol{u} \cdot \boldsymbol{n} = 0, \tag{13}$$

where C is the sliding coefficient. Periodic BC for the inlet/outlet are used, such that the velocity, pressure and specific enthalpy are the same on both ends. On the side boundaries of the domain,

150 symmetry for velocity and thermal insulation are imposed:

$$\boldsymbol{u}_{in} = \boldsymbol{u}_{out} \qquad p_{in} = p_{out} \qquad H_{in} = H_{out}, \tag{14}$$

$$\boldsymbol{K} = [\mu(\nabla \boldsymbol{u} + (\nabla \boldsymbol{u})^T)]\boldsymbol{n}, \qquad \boldsymbol{K} - (\boldsymbol{K} \cdot \boldsymbol{n})\boldsymbol{n} = 0, \qquad \boldsymbol{u} \cdot \boldsymbol{n} = 0, \tag{15}$$

155 $$-\boldsymbol{n} \cdot \nabla H = 0, \tag{16}$$

At the surface, a value is set for specific enthalpy (H_s) corresponding to a surface temperature of $T_s = -30\,^\circ\mathrm{C}$ ($W_s = 0$,$p_s = 0$) such that:

$$H_s = H_i + c(T_s - T_m), \tag{17}$$

At the base, the geothermal flux (q_{geo}) is used for cold ice and a zero flux for temperate ice:

160 $$\boldsymbol{n} \cdot \left(\left\{ \begin{array}{c} -K_i \nabla H \\ -K_0 \nabla H \end{array} \right\} \right) = \left\{ \begin{array}{c} q_{geo},\, if\, T < T_m \\ 0,\, if\, T = T_m \end{array} \right\}, \tag{18}$$

where H_i is the specific enthalpy of pure ice at the melting temperature. To correctly determine the basal boundary condition for the enthalpy field equation, a switching between a Dirichlet and a Neumann condition is necessary (Aschwanden et al., 2012; Kleiner et al., 2015), which depends on basal temperature, water availability at the base and whether a temperate layer exists or not
165 immediately above it. Here we opt for a simpler, more computationally efficient boundary condition where the geothermal flux is gradually decreased in the specific enthalpy range corresponding to $[(T_m - 0.2\,^\circ\mathrm{C}) \quad (T_m)]$, with a smoothed Heaviside function with continuous derivatives.

For the age-depth relation (Eq. 9), periodic boundary conditions are used for the inlet and outlet. At the surface, the age is set to $\chi_s = 0$. Zero normal fluxes are used for the side boundaries and the
170 lower boundary.

$$-\boldsymbol{n} \cdot (-\nabla \chi) = 0, \tag{19}$$

Computational domain

We define the computational domain as a rectangular box 350 km long and 100 km wide with a fixed
175 bed slope (α). The ice thickness is set to 1500 m and three different lakes sizes are used, based on typical sizes of subglacial lakes found in Antarctica (Siegert et al., 1996; Siegert and Kwok, 2000). The lakes are all elliptical in shape, with major and minor axes defined in Table 2. The major axis

Table 1: Values for constants used in the study

	Constants	values
α	bed inclination	$0.3\,^{\circ}$
ρ	density of ice	$910\,\mathrm{kg/m^3}$
g	gravitational acceleration	$9.81\,\mathrm{m/s^2}$
n	flow law exponent	3
γ	Clausius-Clapeyron constant	$9.8 \cdot 10^{-8}\,\mathrm{K/Pa}$
${T_m}^0$	melting point at atm.pressure	$273.15\,\mathrm{K}$
A_0	pre-exp. constant ($T \leq 263.15\,\mathrm{K}$)	$3.985 \cdot 10^{-13}\ \mathrm{s^{-1}Pa^{-3}}$
	- ($T > 263.15\,\mathrm{K}$)	$1.916 \cdot 10^{-3}\ \mathrm{s^{-1}Pa^{-3}}$
Q	activation energy ($T \leq 263.15\,\mathrm{K}$)	$60\,\mathrm{kJ/mol}$
	- ($T > 263.15\,\mathrm{K}$)	$139\,\mathrm{kJ/mol}$
R	universal gas constant	$8.3145\,\mathrm{J/(mol \cdot K)}$
k	thermal conductivity	$2.1\,\mathrm{W/(m \cdot K)}$
c	heat capacity	$2009\,\mathrm{J/(kg \cdot K)}$
L	latent heat of fusion	$3.35 \cdot 10^5\,\mathrm{J/kg}$
d_χ	diffusion coefficient	$10^{-13}\,\mathrm{m^2/s}$
C	friction coefficient	$10^{13}\,\mathrm{(s \cdot m^2)kg^{-1}}$
H	ice thickness	$1500\,\mathrm{m}$
a_s	surface accumulation	$0\,\mathrm{m/s}$
T_s	surface temperature	$-30\,^{\circ}\mathrm{C}$
q_{geo}	geothermal flux	$55\,\mathrm{mW/m^2}$
η_{const}	ice viscosity (constant)	$10^{14}\,\mathrm{Pa\,s}$

Table 2: Values for lake sizes used in the paper

Lake size	Major axis	Minor axis
L_S	10 km	5 km
L_M	20 km	10 km
L_L	30 km	15 km

is aligned with the direction of flow. The model experiments are all either steady state solutions or start from steady state solutions.

Throughout the domain, extruded triangular (prismatic) elements are used with a horizontal resolution down to $\sim$500 m at the lake edges. This relatively high resolution is needed in order to capture

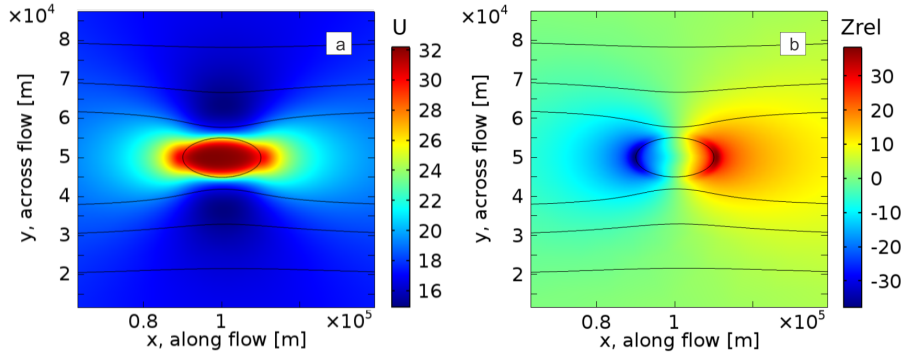

(a) Horizontal velocity, U [m/a] (b) Relative surface elevation, Zrel [m]

Figure 1: 2D surface plots of horizontal velocity (a) in [m/a] and relative surface elevation (b) in [m]. The outline of the lake and streamlines are shown in black and flow is from left to right.

the effect of strain softening of ice around the lake edges where velocity gradients are large and to properly resolve the upper surface. The model uses 15 vertical layers, which become thinner towards the base, where the thinnest layer has a thickness of $\sim 35\,\mathrm{m}$.

3 Model experiments

The aim of the study is to show how ice dynamics and the thermal evolution are affected by the presence of a subglacial lake and to follow its effect on the internal layering through simple temporally dependent and steady state experiments.

All transient simulations are started from an initially steady-state configuration, where equations for mass, momentum, and enthalpy are solved jointly with a direct solver along with equations for surface or grid evolution.

The lake itself is modelled as a "slippery spot" (Pattyn et al., 2004; Sergienko et al., 2007). The lake surface is assumed to be fixed to the bed plane. In reality, any changes to lake size or volume would lead to vertical movement of the lake surface, which in itself would induce an expression at the surface of the ice. For such a scenario, the strongest effect would be experienced by the internal layers closest to the bed (Sergienko et al., 2007). Here we consider only planar changes in lake geometry, or changes in lake size fixed to the bed plane.

The lack of basal friction over the lake results in increased velocities, not just over the lake but also a considerable distance both upstream and downstream of the lake location. Figure 1a shows the surface velocity with black lines indicating streamlines and Figure 1b shows the relative change in surface elevation caused by the presence of the lake, where the general slope has been subtracted from the surface. The surface responds to the change in basal conditions by becoming flatter and with more than a doubling of horizontal velocities over the lake. Streamlines contract and ice is brought in towards the lake from the sides.

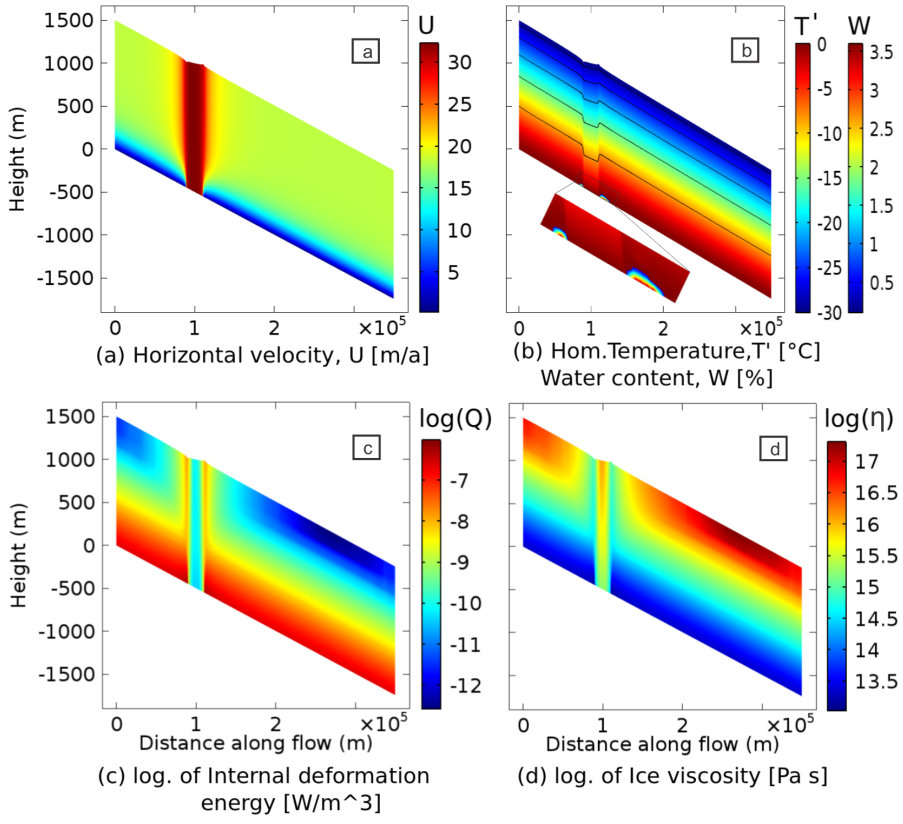

Figure 2: Cross-sectional plots in the flow direction, through the center of the lake. (a) shows horizontal velocity in [m/a]. (b) shows the homologous temperature in $^{\circ}C$ and water content in percentage. The inlet figure shows a close-up of the temperate layers at the lake edges. In (c) we see the logarithm of the internal deformation energy [W/m^3] while (d) shows the logarithm of the viscosity [Pa s]

Figure 2 shows vertical cross sections, through the center of the lake, in the direction of flow for the L_M lake size and different lake parameters. Over the lake, the ice basically moves as an ice shelf with more or less uniform horizontal velocity throughout the ice column (Fig. 2a). At the upstream end of the lake, a strong downward movement of ice causes cold ice from the upper layers to be drawn down towards the bottom, steepening the temperature gradient close to the base. Conversely, at the downstream end a strong upward flow restores internal layers to their prior depths, before the influence of the lake is felt.

The temperature and microscopic water content within the ice are shown in Fig. 2b. Black lines represent stream-lines which coincide, or line up, with isochrone layers for steady-state simulations (Hindmarsh et al., 2006).

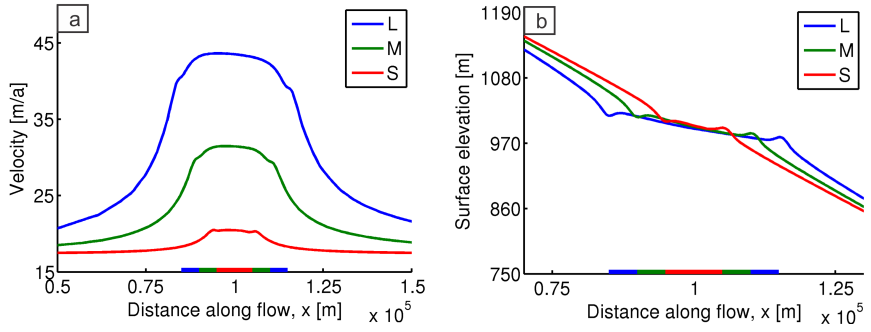

Figure 3: Surface velocity (a) and elevation (b) across the lake, in the flow direction. Velocity and surface profiles for the different lake sizes (L, M, S) are marked with different colors and the horizontal extent of each lake is marked with a vertical bar at the bottom. Note the different horizontal scale for the two figures.

The intense internal deformation close to the borders of the lake, where ice velocities change significantly over short distances, gives rise to a thin temperate layer of ice at both the upstream and downstream ends of the lake (Fig. 2b).

Figure 2c shows the internal deformation energy, with high values near the base where velocity gradients are high. Maximum values are reached near the edges of the lake, in the transition zone between low and full sliding.

Increases in temperature, pressure, water content and larger effective stress all have the effect of decreasing the viscosity, which is why the lowest viscosity values are obtained at the base of the ice sheet, in particular around the edges of the lake (Fig. 2d). Generally low viscosity is furthermore obtained throughout the ice column over the lake boundary, extending all the way up to the surface, effectively creating a vertical zone of softer ice.

Figure 3a shows profiles of horizontal surface velocity for the three different lake sizes considered. As expected, velocity peaks over the lake surfaces and two fringe peaks at the lake edges are discernible for the smallest lake size as well.

A characteristic surface dip feature is observed at the upstream end of many lakes in Antarctica, for instance the Recovery Lakes (Bell et al., 2007; Langley et al., 2011) and Lake Vostok (Studinger et al., 2003) as well as a small hump at the downstream end. Figure 3b shows surface profiles for the three different lake sizes, each with the characteristic flattening of the surface as well as the dip and ridge features on each side of the lake.

Figure 4a shows a comparison of surface profiles for the L_M lake size, made with a constant ($\eta_{const} = 10^{14}$ Pa s) versus a nonlinear viscosity ($n = 3$ in Glen's flow law) and a pressure and temperature dependent one ($n = 1$) but otherwise using the same setup. The hummocky feature is noticeably absent from simulations with a constant viscosity. Figure 4b and 4c show vertical profiles,

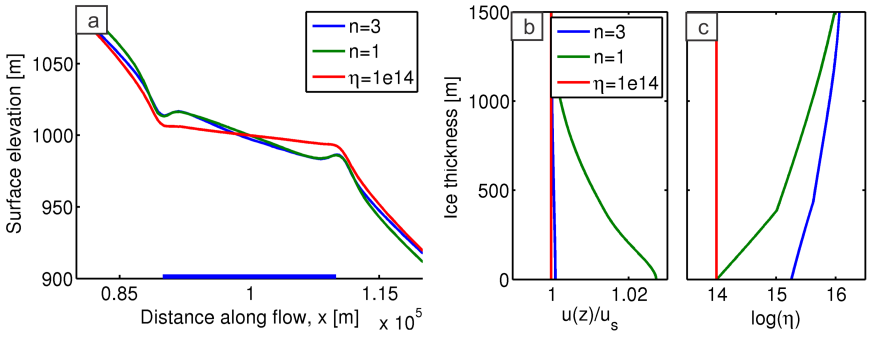

Figure 4: (a) Profiles of surface elevation in [m] for the L_M lake size and three different viscosity cases; fixed viscosity ($\eta_{const} = 10^{14}\,\mathrm{Pa\,s}$), with flow exponent $n = 1$ and $n = 3$ in Glen's flow law (Eq. 4). (b) Scaled horizontal velocity and (c) the logarithm of ice viscosity, in a vertical profile over the center of the lake. The horizontal velocity has been scaled with the velocity magnitude at the surface.

over the center of the lake, of horizontal velocity and viscosity for the three different viscosity cases. The horizontal velocity has been scaled with the horizontal velocity at the surface (the uppermost point of the vertical profile). For both the $n = 1$ and $n = 3$ cases, the horizontal velocity at depth is larger than at the surface.

Lakes drain and fill on different time scales. Several studies have documented relatively rapid drainage events in subglacial lakes in Antarctica (Gray et al., 2005; Wingham et al., 2006; Bell et al., 2007). Typically, drainage occurs over the course of several years but take much longer to refill. To simulate such an event and what effect it could have on the internal structure of the ice, we set up a model run where the lakes diameter shrinks during a 10 year period from the maximum (L_L) to the smallest lake size used in the paper (L_S). Figure 5 shows four different time slices of horizontal velocity, with black lines indicating isochrone layers. As the velocity field adjusts in time to the new boundary conditions, a travelling wave is created at depth within the isochrone structure that transfers downstream with the flow of ice.

4 Discussion

The frictionless boundary levels the surface over the lake, changing surface gradients and causing the ice to speed up in the vicinity of the lake. The increase in velocity is further amplified by the effect of velocity gradients on ice viscosity. Outside the lake, the velocity field is primarily affected by changes in surface gradients and longitudinal stresses and, to a lesser degree, by changes in ice viscosity and basal velocities. Over the lake, the ice moves more like an ice shelf, with almost uniform horizontal velocity throughout the ice column. The increase in velocity (Fig. 2a) is due to

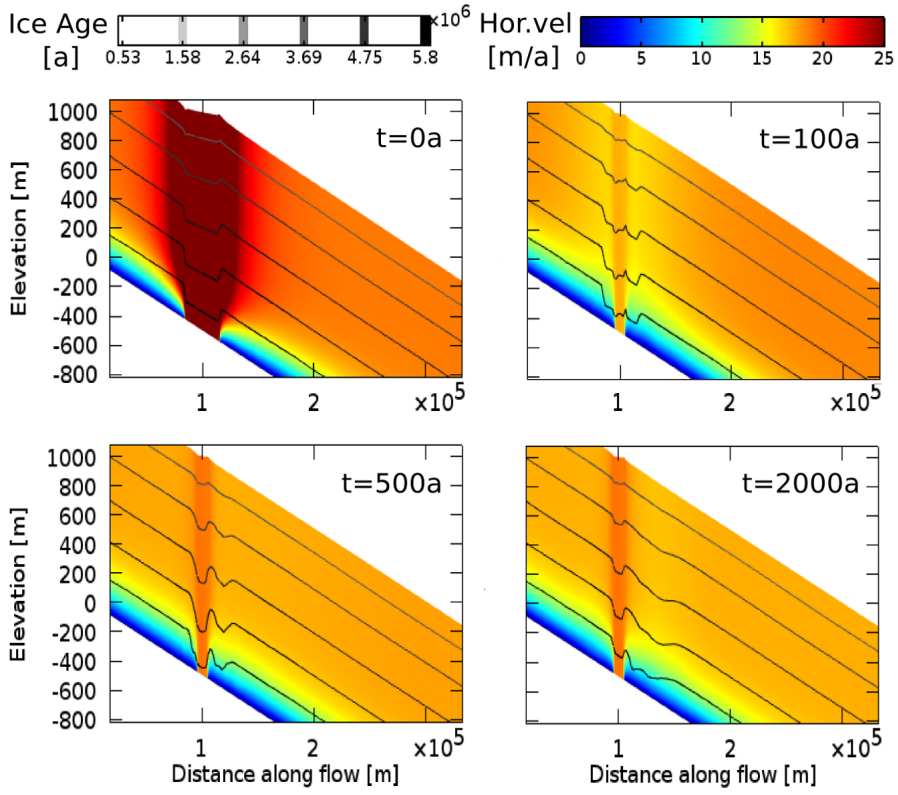

Figure 5: Four different time slices of the velocity and isochrone adjustment to a drainage event. The color scale represents horizontal velocity [m/a] and yellow and black lines indicate streamlines and isochrones respectively. (a) represents the initial stage ($t = 0$), (b) a 100 years later ($t = 100a$), (c) $t = 500a$ and (d) $t = 2000a$.

the lack of basal friction over the lake, causing the highest velocities to appear there but secondary velocity peaks (Fig. 3) can also be discerned at the lake edges, which result from the interaction of surface evolution and ice dynamics. The velocity increase for the two fringe peaks propagates from the surface and downward whereas the velocity peak over the lake is mostly caused by acceleration in the basal layers of the ice sheet.

Thermal regime

For the given model setup, the geothermal flux is sufficient to ensure that the basal temperature reaches the pressure melting point everywhere in the model. Internal deformation then raises the specific enthalpy in the vicinity of the lake, effectively creating a thin layer ($\sim 70\,\mathrm{m}$, 2 vertical cells) of temperate ice with non-zero microscopic water content (Fig. 2b). The steeper temperature gradient over the lake efficiently leads away excess heat created by internal deformation at the upstream end, refreezing whatever microscopic water created upstream. Large quantities of microscopic water, in

reality, would drain to the base ($\sim > 3\,\%$), although drainage is not included here as water content is relatively low.

Two factors would contribute to facilitating freeze-on at the interface between ice and lake water, if it were included in the model. First, draw-down of cold ice from the surface increases the temperature contrast in the lower part of the ice sheet, second, heat from internal deformation ceases with the removal of basal traction over the lake surface. Both result in a steepening of the temperature gradient close to the base, which more efficiently removes heat from the base and shifts the balance in favour of freeze-on.

As lake size increases so too do horizontal velocities over the lake (Fig. 3), as well as the effective strain rates and as a result, the thickness of the temperate layer at the lake boundaries also increases. Accretion rates at the ice/lake interface would be limited by the amount of latent thermal energy that the ice above it can efficiently lead away and any temperate layer formed by internal deformation at the lake boundary would, during its existence, block heat flow and thus accretion, until it completely refroze first. In addition, the larger the lake, the further down cold ice from the upper layers of the ice sheet are advected, further increasing the temperature contrast at depth.

Transition zone

The softening effect of local increases in effective stress at the lake edges, effectively creates a vertical layer of soft ice in between, higher viscosity ice (Fig. 2c). Strong vertical flow at the edges of the lake results from the localized lack of basal traction. A clear difference can be seen between simulations with constant viscosity and viscosity that depends on pressure and temperature (Fig. 4). The softening effect of increasing temperature and pressure with depth not only causes velocity changes in the vertical to be concentrated in the lower layers of an ice sheet but also means that for areas with varying basal traction, such as subglacial lakes, that the ice at depth will support less lateral shear and longitudinal stresses compared to the upper layers where viscosity is higher. This in return means that as the ice encounters a slippery spot or a spot with a sharp decrease in basal traction, such as a subglacial lake, that the force balance will be different than in the isotropic case, where viscosity is everywhere the same. The imbalance in mass flux at depth must be compensated by a more localized increase in vertical flow and a subsequent drop in surface elevation at the upstream side and an upwelling at the downstream side of the lake due to the limited vertical extent of a typical ice sheet.

For large subglacial lakes, where the basal traction is zero, the horizontal velocity at depth is predicted to be slightly larger (here about $0.1\,\%$ for $n = 3$, Fig. 4b) than at the surface. Lakes, such as subglacial lake Vostok, should therefore experience extrusion flow at the base, where the basal horizontal velocity exceeds that at the surface. Extrusion flow is not a requirement though for the formation of these dip and ridge features, as it is sufficient to have a sharp transition in sliding veloc-

ity along with a weaker lower layer to form them and they are predicted to form as well for situations where there is simply a strong decrease in basal traction, not necessarily a complete disappearance.

Drainage experiment

Drainage cycles in Antarctica, cycles including both draining and filling i.e., can have frequencies on decadal to centennial time scales or potentially even larger (Pattyn, 2008; Wingham et al., 2006). Although the drainage takes course during 10 years here, it can be seen as instantaneous given the generally slow flow of ice. The velocity field adjusts rather rapidly ($\sim 100a$) to the new basal boundary conditions relative to the time it takes for the isochrones to respond as the flow of ice is relatively slow. For episodic drainage cycles, the strength of the response will partly depend on how long it takes for the lake to refill.After roughly 2000 years, the wave has moved far enough downstream to be more or less separated from its initial location (Fig. 5d). As both the upstream and downstream lake boundaries move during the drainage event, a two-troughed wave is created. In draining lakes where one end is much deeper than the other a single wave would be expected, as only the shallower end is likely to move significantly. The velocity of the moving boundary also effects the amplitude of the resulting isochrone disturbance (Wolovick et al., 2014), where a slip boundary, moving with the ice, is capable of distorting isochrone layers to a much greater extent than stationary slip boundaries. For maximum effect, the boundary should be moving at a velocity comparable to the averaged ice column velocity.

Water in very active subglacial systems, such as recently discovered in West Antarctica (Gray et al., 2005; Fricker et al., 2007) has relatively short residence times and fast circulation, contrary to previous beliefs. The impact of such short drainage cycles, where both drainage and refilling happen on decadal time scales, is unlikely to have a strong effect on the internal isochrone layers as it takes a long time for the ice to respond. Regular drainage events in subglacial lakes that have a much shorter cycle than the time it takes for a particle of ice to be brought up by vertical flow at the edge of the lake, will therefore probably not be easily detectable in the isochrone structure. If the frequency of drainage cycles is high, the ice will have little time to respond and the amplitude of the resulting wave will be small. Drainage of large lakes in areas with low basal melt rates and consequently long filling times on the other hand could be expected to generate travelling waves, downstream of the lake, with a sufficiently large amplitude to be detectable within downstream isochrones. The amplitude of the travelling wave would be expected to be similar in magnitude as the steady state isochrone disturbance over the lake itself (Fig. 5). Here, on the order of $\sim 100\,\mathrm{m}$ at depth, well within the bounds of being measurable by modern radar systems. As layer stratigraphy is often quite complex, a numerical model of ice age and velocities would be needed to separate the effect of temporally changing lake size, or basal conditions, from layer deflections caused by varying basal topography, or rheology.

For our particular setup, the isochrone disturbance, or the travelling wave, should eventually overturn and create a fold as the stress situation downstream of the lake is essentially one of simple shear without any longitudinal extension (Waddington et al., 2001; Jacobson and Waddington, 2005). Resolving this would require an equally fine resolution downstream of the lake, as over the lake itself, so this is not done here. For a subglacial lake situated at the onset of streaming flow, a fold might not be expected though, as overturning would be counteracted by longitudinal extension and vertical compression, which would tend to flatten all layer disturbances. In general, both horizontal shear and longitudinal extension can be assumed to be present and thus, whether a layer disturbance develops into a fold or flattens out, to eventually disappear, will be decided by the balance between the two (Waddington et al., 2001).

5 Conclusions

Subglacial lakes represent areas of the ice sheet base which are incapable of exerting any horizontal stress on the overlying ice. The rapid transition from little to full sliding causes intense deformation, leading to both an increase in enthalpy and strain softening of ice at the lake edges, and can result in the formation of a temperate layer of ice. The decrease in viscosity with depth leads to preferential deformation of the lower layers of an ice sheet which, for subglacial lakes, results in a hummocky surface feature above the upstream and downstream lake edges. These dip and ridge features can be taken as evidence for a rapid transition in basal sliding, with strong vertical movement of ice as a result. Lakes without this feature would be expected to experience a more gradual increase in sliding, approaching the lake, or continued fast flow downstream, as with subglacial lakes at the onset of ice streaming. Over the lake itself, the ice moves more like an ice shelf, with zero basal traction and virtually no internal strain heating. As a result, temperature gradients over the lake steepen, making them more prone to freeze-on at the ice/water interface than other areas of the ice sheet. A rapid decrease in lake size (or basal friction) causes a travelling wave to be created at depth within isochrone layers, suggesting that certain aspects of lake history are preserved within them and could potentially be deciphered from radio echo sounding data downstream of lake locations when combined with output from numerical models.

Acknowledgements. Funding for this work came from the Research Council of Norway (RCN), Statoil, Det Norske ASA and BG group Norway (grant 200672) to the PetroMaks project “Glaciations in the Barents Sea area (GlaciBar)”, and from the Research School in Arctic Marine Geology and Geophysics (AMGG) at the University of Tromsø. This is also a contribution to the Centre of Excellence: Arctic Gas Hydrate, Environment and Climate (CAGE) funded by RCN (grant 223259). In addition, we would like to thank Nina Wilkens and Martin Rückamp for help with getting started with COMSOL, and the STALLO support team for invaluable assistance.

References

Aschwanden, A., Bueler, E., Khroulev, C., and Blatter, H.: An enthalpy formulation for glaciers and ice sheets, Journal of Glaciology, 58, 441–457, 2012.

Bell, R., Studinger, M., Shuman, C., Fahnestock, M., and Joughin, I.: Large subglacial lakes in East Antarctica at the onset of fast-flowing ice streams, Nature, 445, 904–907, 2007.

Bentley, M., Christoffersen, P., Hodgson, D., Smith, A., Tulaczyk, S., and Le Brocq, A.: Subglacial Lake Sediments and Sedimentary Processes: Potential Archives of Ice Sheet Evolution, Past Environmental Change, and the Presence Of Life, pp. 83–110, American Geophysical Union, doi:10.1002/9781118670354.ch6, http://dx.doi.org/10.1002/9781118670354.ch6, 2013.

Christoffersen, P., Tulaczyk, S., Wattrus, N., Peterson, J., Quintana-Krupinski, N., Clark, C., and Sjunneskog, C.: Large subglacial lake beneath the Laurentide Ice Sheet inferred from sedimentary sequences, Geology, 36, 563–566, 2008.

Dowdeswell, J. and Siegert, M.: The dimensions and topographic setting of Antarctic subglacial lakes and implications for large-scale water storage beneath continental ice sheets, Geological Society of America Bulletin, 111, 254–263, 1999.

Duval, P.: The role of the water content on the creep rate of polycrystalline ice, Isotopes and impurities in snow and ice, 118, 29–33, 1977.

Fricker, H., Scambos, T., Bindschadler, R., and Padman, L.: An active subglacial water system in West Antarctica mapped from space, Science, 315, 1544–1548, 2007.

Glen, J.: The creep of polycrystalline ice, Proceedings of the Royal Society of London. Series A. Mathematical and Physical Sciences, 228, 519–538, 1955.

Gray, L., Joughin, I., Tulaczyk, S., Spikes, V., Bindschadler, R., and Jezek, K.: Evidence for subglacial water transport in the West Antarctic Ice Sheet through three-dimensional satellite radar interferometry, Geophysical Research Letters, 32, 2005.

Greve, R.: Application of a polythermal three-dimensional ice sheet model to the Greenland ice sheet: response to steady-state and transient climate scenarios, Journal of Climate, 10, 901–918, 1997.

Greve, R. and Blatter, H.: Dynamics of ice sheets and glaciers, Springer Science & Business Media, 2009.

Hindmarsh, R., Leysinger-Vieli, G., Raymond, M., and Gudmundsson, G.: Draping or overriding: the effect of horizontal stress gradients on internal layer architecture in ice sheets, Journal of Geophysical Research: Earth Surface (2003–2012), 111, 2006.

Hindmarsh, R., Leysinger-Vieli, G., and Parrenin, F.: A large-scale numerical model for computing isochrone geometry, Annals of Glaciology, 50, 130–140, 2009.

Hutter, K.: A mathematical model of polythermal glaciers and ice sheets, Geophysical & Astrophysical Fluid Dynamics, 21, 201–224, 1982.

Jacobson, H. and Waddington, E.: Recumbent folding of divide arches in response to unsteady ice-divide migration, Journal of Glaciology, 51, 201–209, 2005.

Kleiner, T., Rückamp, M., Bondzio, J., and Humbert, A.: Enthalpy benchmark experiments for numerical ice sheet models, The Cryosphere, 9, 217–228, doi:10.5194/tc-9-217-2015, http://www.the-cryosphere.net/9/217/2015/, 2015.

Langley, K., Kohler, J., Matsuoka, K., Sinisalo, A., Scambos, T., Neumann, T., Muto, A., Winther, J., and Albert, M.: Recovery Lakes, East Antarctica: Radar assessment of sub-glacial water extent, Geophysical Research Letters, 38, 2011.

Langley, K., Tinto, K., Block, A., Bell, R., Kohler, J., and Scambos, T.: Onset of fast ice flow in Recovery Ice Stream, East Antarctica: a comparison of potential causes, Journal of Glaciology, 60, 1007–1014, 2014.

Leysinger-Vieli, G., Hindmarsh, R., and Siegert, M.: Three-dimensional flow influences on radar layer stratigraphy, Annals of Glaciology, 46, 22–28, 2007.

Palmer, S., Dowdeswell, J., Christoffersen, P., Young, D., Blankenship, D., Greenbaum, J., Benham, T., Bamber, J., and Siegert, M.: Greenland subglacial lakes detected by radar, Geophysical Research Letters, 40, 6pp, http://doi.wiley.com/10.1002/2013GL058383, 2013.

Parrenin, F. and Hindmarsh, R.: Influence of a non-uniform velocity field on isochrone geometry along a steady flowline of an ice sheet, Journal of Glaciology, 53, 612–622, 2007.

Parrenin, F., Hindmarsh, R., and Rémy, F.: Analytical solutions for the effect of topography, accumulation rate and lateral flow divergence on isochrone layer geometry, Journal of Glaciology, 52, 191–202, 2006.

Pattyn, F.: Investigating the stability of subglacial lakes with a full Stokes ice-sheet model, Journal of Glaciology, 54, 353–361, 2008.

Pattyn, F., De Smedt, B., and Souchez, R.: Influence of subglacial Vostok lake on the regional ice dynamics of the Antarctic ice sheet: a model study, Journal of Glaciology, 50, 583–589, 2004.

Sergienko, O., MacAyeal, D., and Bindschadler, R.: Causes of sudden, short-term changes in ice-stream surface elevation, Geophysical Research Letters, 34, 2007.

Siegert, M.: Antarctic subglacial lakes, Earth-Science Reviews, 50, 29–50, 2000.

Siegert, M. and Kwok, R.: Ice-sheet radar layering and the development of preferred crystal orientation fabrics between Lake Vostok and Ridge B, central East Antarctica, Earth and Planetary Science Letters, 179, 227–235, 2000.

Siegert, M., Dowdeswell, J., Gorman, M., and McIntyre, N.: An inventory of Antarctic sub-glacial lakes, Antarctic Science, 8, 281–286, 1996.

Siegert, M., Le Brocq, A., and Payne, A.: Hydrological connections between Antarctic subglacial lakes, the flow of water beneath the East Antarctic Ice Sheet and implications for sedimentary processes, Glacial Sedimentary Processes and Products, pp. 3–10, 2007.

Steinemann, S.: Results of preliminary experiments on the plasticity of ice crystals, Journal of Glaciology, 2, 404–412, 1954.

Studinger, M., Bell, R., Karner, G., Tikku, A., Holt, J., Morse, D., Richter, T., Kempf, S., Peters, M., Blankenship, D., et al.: Ice cover, landscape setting, and geological framework of Lake Vostok, East Antarctica, Earth and Planetary Science Letters, 205, 195–210, 2003.

Thoma, M., Grosfeld, K., Mayer, C., and Pattyn, F.: Interaction between ice sheet dynamics and subglacial lake circulation: a coupled modelling approach, The Cryosphere, 4, 1–12, 2010.

Waddington, E., Bolzan, J., and Alley, R.: Potential for stratigraphic folding near ice-sheet centers, Journal of Glaciology, 47, 639–648, 2001.

Weertman, J.: Sliding-no sliding zone effect and age determination of ice cores, Quaternary Research, 6, 203–207, 1976.

Wingham, D., Siegert, M., Shepherd, A., and Muir, A.: Rapid discharge connects Antarctic subglacial lakes, Nature, 440, 1033–1036, 2006.

Wolovick, M., Creyts, T., Buck, W., and Bell, R.: Traveling slippery patches produce thickness-scale folds in ice sheets, Geophysical Research Letters, 2014.

Wright, A. and Siegert, M.: A fourth inventory of Antarctic subglacial lakes, Antarctic Science-Institutional Subscription, 24, 659, 2012.

Paper 3

Gudlaugsson, E., Humbert, A., Andreassen, K., Clason, C., Kleiner, T. and Beyer, S.: Eurasian ice sheet dynamics and sensitivity to subglacial hydrology. Manuscript

UiT / THE ARCTIC UNIVERSITY OF NORWAY

Manuscript

Eurasian ice sheet dynamics and sensitivity to subglacial hydrology

Eythor Gudlaugsson[1], Angelika Humbert[2,3], Karin Andreassen[1], Caroline C. Clason[4], Thomas Kleiner[2], and Sebastian Beyer[2]

[1]Centre for Arctic Gas Hydrate, Environment and Climate (CAGE), Department of Geology, UiT – The Arctic University of Norway, Tromsø, Norway
[2]Section of Glaciology, Alfred Wegener Institute Helmholtz Center for Polar and Marine Research, Bremerhaven, Germany
[3]Department of Geosciences, University of Bremen, Bremen, Germany
[4]Department of Physical Geography, Stockholm University, Stockholm, Sweden

Abstract.

Ice stream dynamics are strongly controlled by processes taking place at the basal interface between the ice and the underlying bed. Ice streams are typically underlain by a thin layer of water that both lubricates the base and saturates the sediment, decreasing it's shear strength. The presence of water at the base reduces its ability to resist flow and drastically affects sliding velocities.

Here we study the effect of subglacial water on Eurasian ice sheet dynamics during the last glacial cycle. We do this by incorporating a thin-film model of basal water flow into an existing ice sheet model (SICOPOLIS) and use it to enhance flow in temperate areas. Large parts of the former Eurasian ice sheet were underlain by thick sequences of soft, marine sediments and many areas are imprinted with geomorphological features indicative of fast flow and wet basal conditions. Recent studies have indicated that subglacial hydrology played a crucial role in the relatively fast disintegration of the Eurasian ice sheets.

Basal sliding increases with the amount of available subglacial water in temperate areas and results in significantly lower ice volume and thickness building up over time. With the inclusion of basal water, the ice sheet is typically less extensive during warm periods as the thinner ice is more vulnerable to the higher temperatures at lower altitude. During stable conditions and ice sheet growth, ice sheet extent is generally slightly larger. Minima in the pressure potential, governing water flow, are used as indicators for potential locations of past subglacial lakes and a probability distribution of lake existence is presented based on estimated lake depth and longevity. Rapid changes in total lake storage capacity coincide with major peaks in freshwater production and ice sheet reconfigurations, indicating a substantial increase in availability of subglacial water during deglaciation phases that is not fully captured by numerical models unless dynamic storage is accounted for.

1 Introduction

During the Weichselian glacial period, large parts of the Arctic were ice covered. At it's maximum the Eurasian ice sheet, consisting of both the Barents Sea Ice Sheet (BSIS) and the Fennoscandian Ice Sheet (FSIS), merged with the Celtic ice sheet in the south and extended all the way up the north continental shelf, covering both the Barents and the Baltic Seas (Svendsen et al., 2004a). The closest historical equivalent to the West Antarctic Ice Sheet (WAIS) is the former Barents Sea Ice Sheet. During the Last Glacial Maximum (LGM) the two ice sheets were more or less equivalent in both size and volume but whereas the BSIS completely disappeared, the WAIS endured (Svendsen et al., 2004a; Anderson et al., 2002; Evans et al., 2006). Both ice sheets were based largely below sea level and both had large, dynamic ice streams that drained them (Andreassen and Winsborrow, 2009). The BSIS thus constitutes a close geological analogue to WAIS and it's history can provide important insights into the future evolution of the West Antarctic Ice Sheet. Subglacial hydrology is thought to have played a crucial role in the relatively fast disintegration of the BSIS (Bjarnadóttir et al., 2014; Winsborrow et al., 2010). Subglacial water lubricates the ice base by effectively separating it from the underlying bed and decreasing the area and force of contact between the two. It also penetrates sediments, decreasing their shear strength, mainly by separating sediment particles from one another, making it easier for the sediment to deform (Tulaczyk et al., 2000).

Temperate ice and meltwater are typically found either underneath very thick ice due to the geothermal gradient and the insulating properties of ice or in areas of high deformation and/or frictional resistance such as closer to the margin (Siegert et al., 1996). Any meltwater that forms will be transported from areas of high pressure potential to areas with lower potential. It can flow in **i)** a channelized system through so called Rothlisberger channels (Röthlisberger, 1972) or Nye channels (Nye and Frank, 1973) incised either in ice or bedrock, or it can flow in **ii)** a distributed system such as a thin water film (Weertman, 2010) or a system of linked cavities (Lliboutry, 1968). These two systems behave in a fundamentally different way. For distributed systems, the effective pressure decreases with increasing amount of water as the water pressure approaches the ice overburden (Weertman, 1957). Similarly as with the flow of ice, flow of water generates heat due to viscous dissipation causing the interface between the two to melt. At a certain threshold, the melting due to the turbulent energy of the flowing water outweighs the inward creep of the overlying ice (Flowers, 2015; Bell, 2008) and forms a channel. Water discharge through the subglacial hydrological network varies on diurnal time scales or shorter and peak discharge exerts strong control on channel size. Water pressures fluctuate but in general, once a channel has formed it results in increased effective pressures in the surrounding catchment as the water pressures in the channel are usually much lower than in a distributed system. In addition to flow along the ice/bed interface, water can also flow through the sediment where increasing pore water pressures decrease it's yield strength, leading to easier and faster sediment deformation (Tulaczyk et al., 2000).

Rapidly moving corridors of ice, ice-streams, typically move mostly by either basal slip or by deformation of the underlying sediments, both of which are highly dependent on the availability of subglacial water. In modern day ice sheets, up to 90% of mass is lost through these fast flowing corridors of ice (Bamber et al., 2000). Inclusion of these processes in numerical ice sheet models is therefore of vast importance for the accurate estimation of future ice loss in polar regions and changes in global sea level. Subglacial water additionally places some constraints on ice sheet volume as a well lubricated, slippery bed does not support the same shear stress as frozen ground and thus consequentially a much lower ice sheet volume can exist above it.

By studying the dynamics of extinct ice sheets and how models respond to perturbations in external forcing we can learn much about how modern ice sheets are likely to respond to a changing climate and also how much of the dynamics are due to internal changes such as thermodynamical flow switching and other instabilities and how much are due to changes in external conditions such as climate or varying ocean currents.

1.1 Previous modelling studies

The Eurasian ice sheet has previously been modelled with 3D thermomechanically coupled ice sheet models such as the one by Payne and Baldwin (1999) who established a connection between fan-like landform assemblages on a hard-rock area of the Baltic Shield and past ice streaming in the area. Although neither taking into account the Barents Sea part nor subglacial sliding in general, their model output matched reasonably well with available empirical data of the time. Available geological and geophysical data from the former Eurasian Ice Sheet as a whole were later summarized and used for a geological reconstruction of the Quaternary ice sheet development (Svendsen et al., 2004b, a). As part of the same program, the Quaternary Environment of the Eurasian North (QUEEN), Siegert and Dowdeswell (2004) used an inverse modelling approach to simulate the Eurasian ice sheets growth and decay, during the late Weichselian, matching the geological evidence presented. They varied climatic inputs in order to optimize the fit between model evolution and empirical data. Another modelling approach was adopted by Forsström and Greve (2004) who used the shallow ice approximation (SIA) numerical model, SICOPOLIS (Simulation COde for POLythermal Ice Sheets), as we do in this study. In order to adapt their model to empirical data they introduced LGM anomalies in temperature and precipitation forcings. They found that strong west-east gradients in temperature and precipitation were necessary in order to reduce the extent of glaciation in the eastern part, over the Kara Sea and the Pechora lowlands. SICOPOLIS was again used by Clason et al. (2014) who improved upon previous models by incorporating a parametrization of surface meltwater enhanced sliding. They produced a model fitting well with empirical data and again confirmed the necessity of strong west-east gradients in both temperature and precipitation to reduce glaciation in the east.

Here, we further build upon the Clason model, introducing a simple representation of the subglacial hydrological system and examine the influence of subglacial water enhanced sliding on ice dynamics and the temporal evolution of the Fennoscandian and the Barents Sea Ice sheets. In addition, we use the hydrological model to deduce probable locations of past subglacial lakes, their temporal perseverance, size and probability of existence.

2 Modelling approach

2.1 Ice sheet model

We use the thermodynamically coupled ice sheet model SICOPOLIS (Greve, 1997) in order to simulate the Fennoscandian (FIS) and the Barents Sea Ice sheets (BSIS). SICOPOLIS is a fully 3D, polythermal, two-layer model (temperate and cold ice) that uses a simplified set of equations (shallow ice approximation, SIA) to calculate ice velocities, thickness, age, temperature and water content. Ice is treated as an incompressible fluid where strain rates are related to deviatoric stresses via Glen's flow law (Glen, 1955). Ice viscosity depends on the temperature, water content and effective stress at each point. The SIA is incapable of correctly reproducing ice streams as higher order stresses are neglected although it can mimic their effect through enhanced sliding in temperate regions. Large-scale behaviour of ice sheets is generally well represented however.

Isostatic adjustment follows the local-lithospere-relaxing-asthenosphere (LLRA) approach where an ice load causes a local displacement of the lithosphere, balanced by a buoyancy force of the viscously deforming asthenosphere. A more detailed description can be found in Greve and Blatter (2009).

Ice shelves are not treated explicitly, but instead the model is allowed to glaciate the seafloor above a certain threshold depth (1000 m). When ice moves into deeper water, ice thickness is set to zero which can be considered as a crude form of calving. Sensitivity studies show little dependence on this threshold depth, with the main differences between this and the typically used lower threshold of 500 m being that a small area within the North Sea resists glaciation for smaller values (Clason et al., 2014).

2.2 Climate forcing

We employ the same climatic forcing as in Clason et al. (2014) where climatic conditions were linked to the NorthGRIP δ^{18}O ice core record and a synthetic Greenland ice core record based on Antarctic data and the thermal bipolar seesaw model (Wolff et al., 2010; Andersen et al., 2006; Barker et al., 2011). Temperatures and precipitation were scaled between present day and LGM conditions using a combination of CFSR (Climate Forecast System Reanlaysis) data for present-day conditions (Uppala et al., 2005; Saha et al., 2010; Dee et al., 2011) and IPSL (Institut Pierre Simon Laplace) CM5A-LR for LGM conditions (Kageyama et al., 2013). In order to get a realistic ice-sheet extent, comparable

to that compiled by Svendsen et al. (2004a), a linear gradient, from the west to the east, on the LGM temperature data was imposed, reducing temperatures in the west and raising them in the east. For further details see Clason et al. (2014)

2.3 Subglacial hydrology

Following (Kleiner and Humbert, 2014) we use a subglacial water-flow model where water is assumed to flow in a thin film between the underlying substrate and the ice (Le Brocq et al., 2009; Johnson and Fastook, 2002). The time dependent water depth (d) is given by:

$$\frac{\partial d}{\partial t} = M - \nabla \boldsymbol{u_w} d \tag{1}$$

where M is the basal melt rate, computed at every time step, and $\boldsymbol{u_w}$ is the depth-averaged water velocity. A second equation relating water depth, velocity and differences in water pressure can be obtained by assuming that the flow can be described as laminar flow between two parallel plates (Weertman, 1972).

$$\boldsymbol{u_w} = \frac{d^2}{12\mu} \nabla \Phi \tag{2}$$

where μ is the viscosity of the water and Φ the hydraulic potential, which can be written in terms of water pressure (p_w) and an elevation potential (Shreve, 1972).

$$\Phi = \rho_w g z_b + p_w \tag{3}$$

where ρ_w is the density of water, g the gravitational acceleration and z_b is the height of the bedrock relative to some fixed datum.

Water pressure can in turn be described by the ice overburden pressure minus the effective pressure (N). In most cases the effective pressure will be close to zero and the ice effectively 'floating' on top of the water layer.

$$p_w = \rho_i g H - N \tag{4}$$

Here, we assume that the effective pressure is everywhere equal to zero, wich simplifies the pressure potential to a purely geometrical equation where the potential gradient is described as a function of the surface and the bedrock gradient

$$\nabla \Phi = \rho_i g \nabla z_s + (\rho_w - \rho_i) g \nabla z_b \tag{5}$$

where z_s represents the surface. We see from Eq. 5 how important the surface gradient is in governing the subglacial flow of water, or roughly 11 times more important than the bedrock gradient.

It is assumed that the timescales governing water flow are much shorter than those governing the flow of ice and that Eq. 1 thus reaches steady state within each timestep of the ice flow model. Water fluxes are calculated recursively starting from the top of the hydraulic potential surface, in the direction of the hydraulic gradient following Budd and Warner (1996). For an overview of different, typically used flux routing numerical schemes see Le Brocq et al. (2006).

2.4 Basal sliding

We employ a Weertman-type sliding law that relates the basal shear stress and velocity (Weertman, 1957).

$$\boldsymbol{u_b} = -C_b|\tau_b|^{p-1}{\tau_n}^{-q}\boldsymbol{\tau_b} \tag{6}$$

where $\boldsymbol{u_b}$ is the basal velocity, τ_b the basal shear stress and τ_n basal normal pressure which is taken to be equal to the ice overburden. The sliding law is extended in order to allow for sliding at sub-melt temperatures and the thickness of the water layer (H_w) following Kleiner and Humbert (2014) and Johnson and Fastook (2002).

$$C_b = (1+f_w){f_T}{C_b}^0, \qquad \text{and} \qquad f_w = S_w\left[1-exp(-\frac{H_w}{{H_w}^0})\right] \tag{7}$$

where $f_T = exp(\nu(T-T_{pmp}))$, ν is the sub-melt sliding parameter, T temperature, T_{pmp} pressure melting point, ${C_b}^0$ is a basal sliding parameter that depends for example on bed material and roughness, (${H_w}^0$) is a typical scale of water layer thickness (here equal to $1\,mm$) and $S_w + 1$ is the maximum increase in sliding velocity due to subglacial water. Here, we test three different values for S_w, [0, 2, 5] representing a maximum of a six fold increase in sliding velocity due to the water layer (when $S_w = 5$).

2.5 Subglacial lakes and channels

Model output, such as basal meltrates, temperature, ice thickness and isostatic adjustment are interpolated onto high resolution grids, in a post-processing step, and used along with modern day topographic maps of the study area (General Bathymetric Chart of the Oceans (GEBCO),Weatherall et al. (2015)) for high resolution calculations of meltwater routing. These can be used to infer possible locations of subglacial lakes and their temporal duration. Before routing is calculated, any local minima in the hydraulic potential need to be filled to brink, allowing water to continue further downstream. These local minima represent areas where subglacial water would be likely to pond on it's way down the hydraulic potential. By mapping these out we get an idea of potential locations where

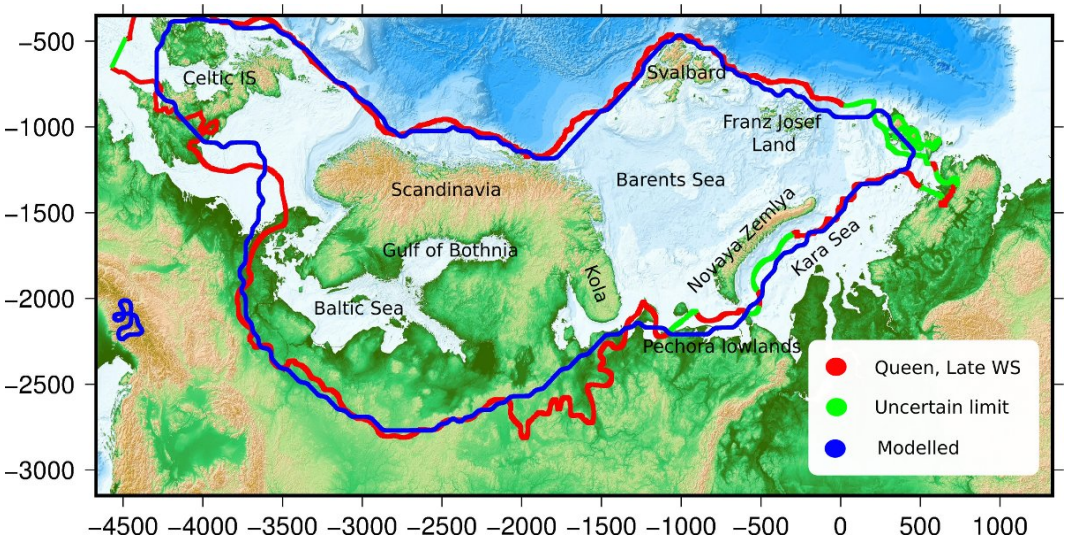

Figure 1: A map showing the study area as well as the modelled and reconstructed extent of the Eurasian ice sheet during at the LGM. The reconstructed extent based on geological evidence from Svendsen et al. (2004a) is shown in red with uncertain limits in green and modelled extent is shown in blue (for $S_w = 5$).

subglacial lakes might have existed in the past and by looking at a selection of time slices we get a sense of how long they were likely to have persisted throughout changes in the ice sheet geometry. By assuming either a fixed surface or a fixed ice thickness, we can calculate back from the filled up potential, the distance that the lower boundary has to be adjusted in order to flatten out the hydraulic potential, with a factor of 11 roughly differentiating the two estimates. This enables us to get a rough approximation of water storage capacity in subglacial lakes. Such a value is unlikely to be of high accuracy, but relative changes in lake storage capacity with time might be considered to be more reliable. Although a water-film model is incapable of reproducing channels in a physically meaningful manner, areas where flow of meltwater converges to form a thick water layer can be considered to be likely locations where channels would have formed in the past.

3 Model results

The model was run for 250 ka to allow for sufficient spin-up time and to minimize any errors arising from arbitrarily chosen initial conditions. Here we present results from the last 100 ka with a focus on the final 30 ka of the Weichselian.

The model results in a two-peaked glacial maximum, with the latter peak occurring around 23.5ka when both area and volume are at a maximum. We will refer to this peak as the LGM. The ice sheet extent at the LGM matches well with empirical data (Fig. 1) with relatively small differences in

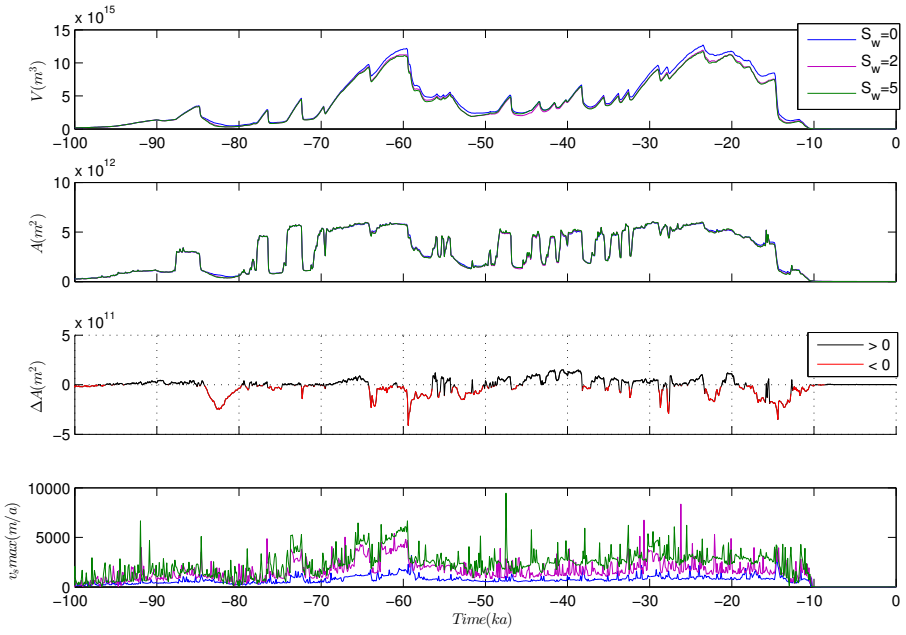

Figure 2: Comparison between simulations with different values of the sliding parameter S_w for the last 100ka. Blue in subfigures (a,b,d) represents simulations without HC sliding ($S_w = 0$), purple $S_w = 2$ and green $S_w = 5$. (a) shows total ice volume in m^3, (b) shows total area coverage of glacial ice in m^2, (c) shows the difference in total area between simulations with ($S_w = 5$) and without ($S_w = 0$) a thin water film. Black denotes points in time when areal coverage is larger for simulations without HC sliding and red otherwise. (d) shows maximum horizontal velocity in (m/a) obtained at each point in time.

extent between model runs with or without water enhanced sliding. Maximum thickness of 4125m is reached slightly later, or at 19ka for simulations with hydrology-coupled (HC) sliding. Maximum horizontal velocities hover around 3000 m/a for $S_w = 5$ with peak values approaching 10 km/a over short time periods (Fig. 2). At the LGM, 20% of the ice sheet base is estimated to be temperate, mostly close to the margin in ice streaming areas. The coldest part of the ice sheet at the LGM, with basal temperatures well below the pressure melting point (-10 - -20) is roughly over Finland, in the center of the domain (Fig. 3). This is also the thinnest part of the ice sheet at that time and therefore the most vulnerable to the cold surface temperatures above. Ice velocities there are close to zero during the LGM and only increase in that area during deglaciation when the ice sheet is smaller and the margin closer.

The model produces two major ice domes that merge around 34ka with one ice dome centring over the Gulf of Bothnia (FSIS) and the other over the Barents Sea (BSIS, Fig. 3a). The Fennoscandian

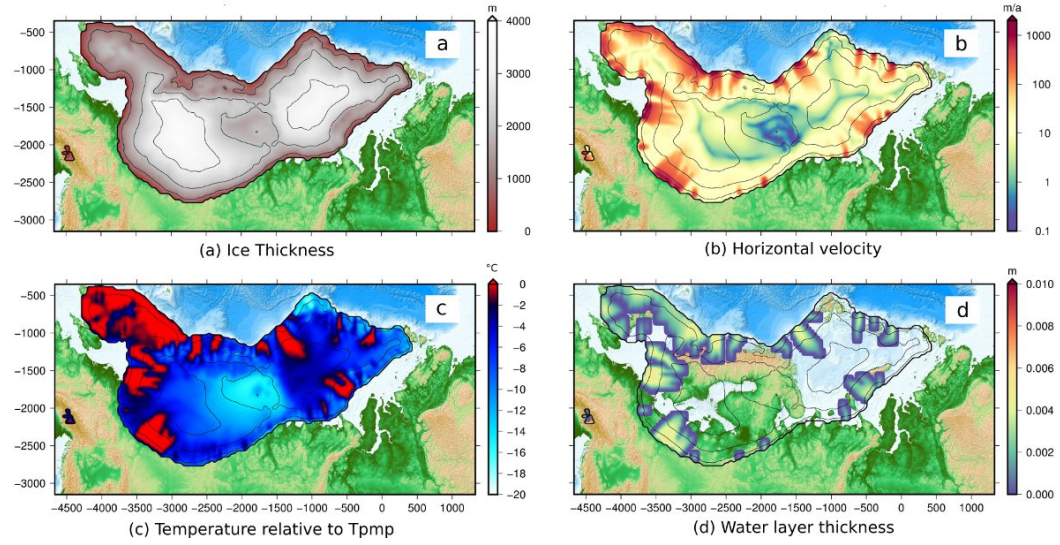

Figure 3: (a) Ice sheet thickness in [m], (b) horizontal velocity in [m/a], (c) basal temperature relative to pressure melting point [°C] and (d) water layer thickness in [m] for the $S_w = 5$ sliding scenario at 23.5ka, the point of maximum ice extent and volume.

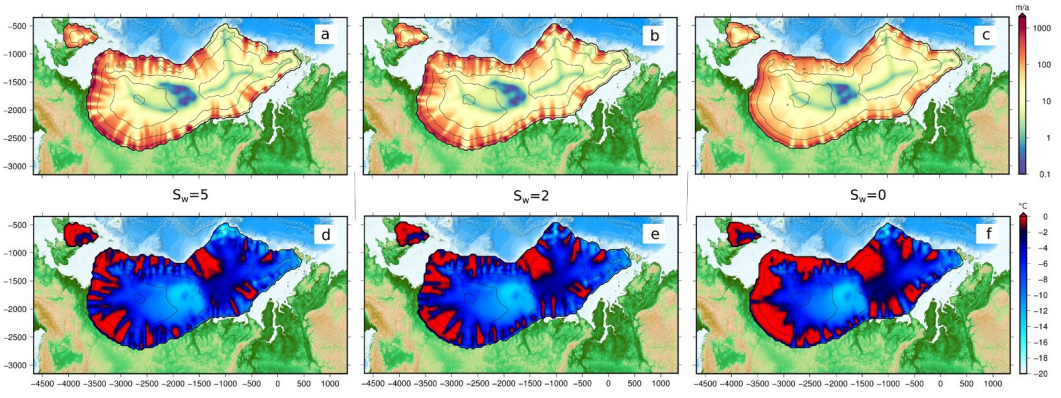

Figure 4: A comparison of horizontal velocity (a,b,c) in [m/a] and temperature (d,e,f) in [$^{\circ}C$] relative to pressure melting point for the three sliding scenarios considered. (a,d) are with $S_w = 5$, (b,e) with $S_w = 2$ and (c,f) without HC sliding ($S_w = 0$)

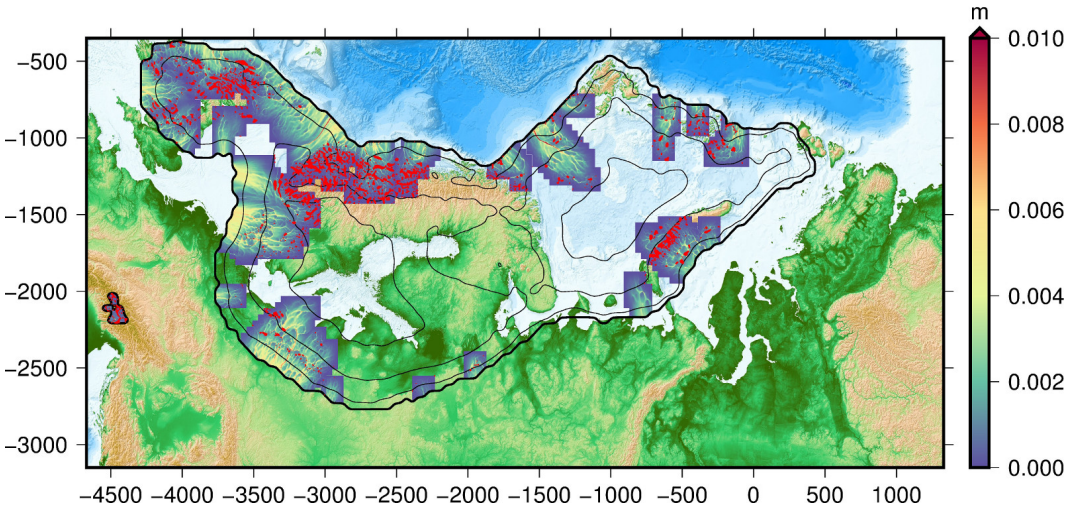

Figure 5: Map of water layer thickness at 23.5ka calculated with a 1km resolution bathymetric grid. Sinks in the hydraulic potential (potential subglacial lakes) are marked with red ($S_w = 5$).

dome then merges with Celtic IS shortly before the LGM, or around 26.5ka to produce one major ice sheet. Whereas many previous numerical studies have typically overglaciated the eastern part of the ice sheet at the LGM, our ice sheet extent in the Kara Sea and the Baltic region matches reasonably well with geological reconstructions (Fig. 1).

Incorporation of HC sliding improves the models ability to mimic ice streams and spatially confine their location. SIA generally produces broad areas of fast flow whereas the inclusion of hydrology-coupled sliding limits and confines fast-flowing areas to temperate areas with a thick water layer (4) and thus better mimics real velocity patterns. The width of ice streaming areas is still somewhat overestimated though because of the limited grid resolution of the numerical model.

No extra bedrock smoothing is applied before melt water is routed along the base to the margin as the 40km grid resolution already represents considerable averaging simply because of the large grid size. The calculated thickness of the water layer used in the model rarely exceeds 6mm. Water is routed along the direction of the largest gradient according to Budd and Warner (1996) and is limited to temperate areas of the ice sheet.

The routing is redone, as a post-processing step, for a selection of time slices every 250 years using modern high resolution bathymetry data (1km grid size) and the calculated ice sheet geometry as well as isostatic adjustment at each time slice. This enables us to estimate possible locations of subglacial lakes as areas of the hydrological potential that represent local minima or sinks. The height to which the sinks need to be adjusted in order to eliminate them is used as a proxy to estimate the potential depth of the subglacial lake, assuming that the change in potential arises solely from a change in water depth. A criterion for the likelihood of a subglacial lake having existed is then

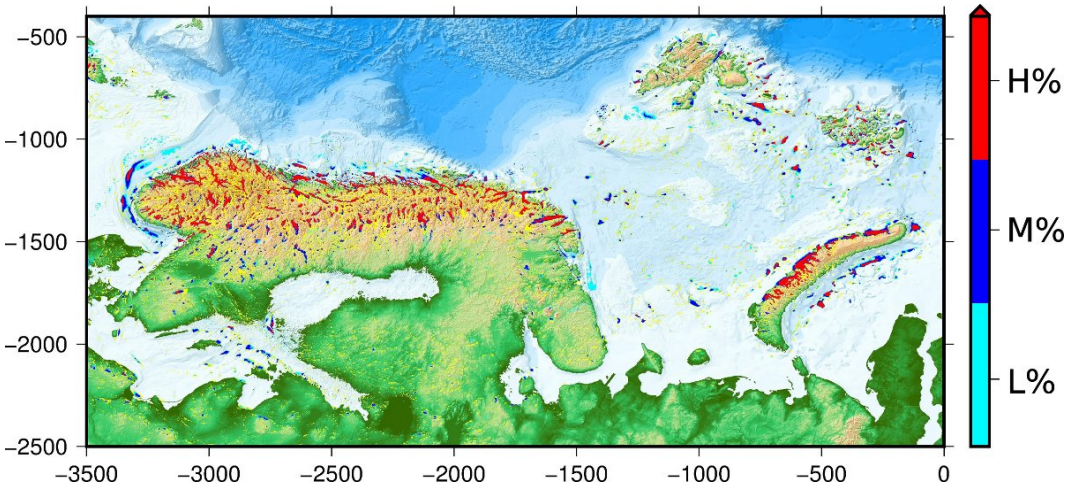

Figure 6: Map showing all predicted lake locations during the period 40ka - 10ka, color-coded based on perceived probability of existence. A deep, temporally persistent lake is deemed as having a higher probability of having existed than a shallow, shortlived one. Calculated with $S_w = 5$.

taken as the product of the depth at each time slice and the time each cell persists as part of a subglacial lake. This is done with a grid resolution of 1km both with and without smoothing (5km) of the underlying bathymetry. Smoothing eliminates mostly small, shallow areas of the hydrological potential that would otherwise show up as potential lakes. For completeness and in order to separate these small shallow areas from the deeper and larger potential lake locations, the routing is calculated without smoothing as well. They are represented by a yellow color in Fig. 6. All grid cells are then ranked with the above criteria, normalized and given a score (H)igh, (M)edium or (L)ow based on the probability of each cell having been part of a subglacial lake, with H representing lakes that are both deep and temporally stable and can thus be considered to be more likely candidates. Each category contains one third of all cells marked as having pertained to a subglacial lake at some point.

By summing up the volume of all lakes for each time slice, a temporal evolution of lake storage capacity can be obtained (Fig. 7). Changes in ice sheet geometry, switches in the thermal regime or deflections of the lithosphere all effect the storage capacity of subglacial water. Here we have opted for the more conservative estimate of lake storage, assuming that any change necessary in the hydraulic potential needed to fill local minima would come from a change in water level alone, leaving ice thickness untouched. This leads to a total amount of stored water of the same order of magnitude as estimated for Antarctica.

4 Discussion

Much like (Clason et al., 2014), the modelled LGM extent of the FSIS and the BSIS matches well with the geological reconstructions of the former ice sheets (Svendsen et al., 2004b, a), with the

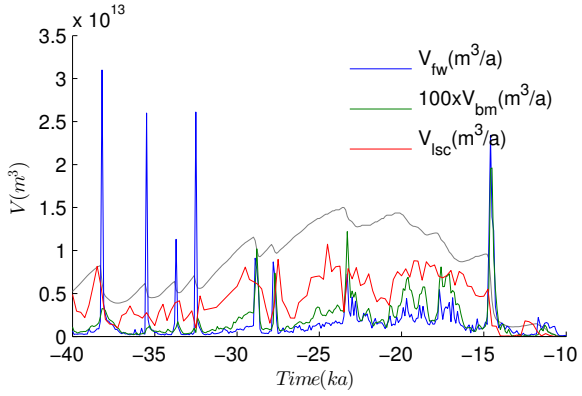

Figure 7: Total freshwater production (V_{fw}), basal melt ($100xV_{bm}$) and lake storage capacity (V_{lsc}) in $[m^3/a]$ from 40ka to 10ka ($S_w = 5$). Ice volume is shown in gray in the background for comparison (not to scale).

inclusion of subglacial hydrology representing a slight improvement both in extent and volume in the Barents Sea region. We have used the same climate forcings as Clason et al. (2014) which along with older work of Siegert and Dowdeswell (2004) and Forsström and Greve (2004) confirmed the need for strong east-west gradients in both temperature and precipitation patterns.

4.1 Hydrology

The meltwater-enhanced sliding has a strong effect on the evolution of the ice sheets. Coupling sliding to the thickness of the water layer increases velocities in temperate, (meltwater-producing) areas and leads to considerably lower ice thickness and volume building up over time. During the early stages of inception little to no differences are seen in either volume or extent as the ice sheet is mostly cold-based. As soon as a part of the margin reaches pressure melting point and sliding picks up, it draws down ice and volume from the surrounding area, deflecting flow directions towards the lowered surface. The total ice sheet extent is not greatly affected by hydrology-coupled (HC) sliding. Most notable are the differences following a warm spell and a sharp decrease in volume where the lower thickness of the hydrology coupled ice sheet means that it is more vulnerable to the higher temperatures at lower altitudes and thus experiences more surface melt and a faster decline. During peak, and ice sheet growth the areal extent is generally slightly larger.

The effect of HC sliding on the basal temperatures, and most notably the percentage of the bed that is actually at pressure melting is greater. As can be seen from figures 2 and 4 a much larger part of the bed is at pressure melting for simulations without subglacial hydrology. When the movement of ice changes from flow by internal deformation to flow by rapid basal sliding, this effects the heat balance of the ice. When basal sliding ensues, heat generated by internal deformation decreases and gets somewhat compensated for by frictional heating between the sliding ice and the underlying

substrate. This however does not explain why models disregarding subglacial hydrology and its effect on sliding would overestimate temperate areas of the ice sheet. The explanation lies in the fact that for the HC sliding scenario, the ice just outside the boundary of temperate ice and rapid sliding will have considerably lower ice thickness and therefore less deformational energy available at it's base for heat generation, in addition to increased advection of colder ice from above. Models neglecting subglacial hydrology are thus likely to overestimate temperate areas of the base as well as volume compared to models that include subglacial hydrology and any associated enhancement in sliding.

4.2 Subglacial lakes

Several subglacial lakes are predicted to have existed during the last glacial cycle (Fig. 6). Particularly in the Norwegian fjords and valleys as well as on the western side of Novaya Zemlya although the bathymetry data on either side of Novaya Zemlya is not of high quality. The island itself represents a significant hydrological barrier to subglacial flow of water with ice flowing generally from the west to the east, over the island, and large parts of the area having a temperate base during much of the glaciation (Fig. 5). Several lakes seem to persist over thousands of years and reach considerable depths. Not many lakes seem to form in the Barents Sea itself, as the bathymetry there is generally quite flat and smooth. The likeliest locations for formation of subglacial lakes in the BS seem to be around Spitsbergenbanken and Central Barents Sea. Many lakes forming there would likely have been 'active' lakes with low water depths, short residence times and fast circulation of water much like lakes in similar settings in West Antarctica (Gray et al., 2005; Fricker et al., 2007). Drainage would be frequent and possibly complete on decadal timescales or slower, in which case the lake roof would come in and out of contact with the underlying sediments, thus complicating the possibility of identifying them today from geological remains. These predictions however, should be taken with precaution as several of the locations could be related to geomorphological features on the seafloor, remainders of the deglaciation of the area, and would therefore not be present in its current form during the time when a subglacial lake is predicted to have formed there. Any detailed analysis of for which lakes this is true and for which it isn't is considered to be outside the scope of this paper.

Subglacial lakes represent areas of the ice sheet base, fixed at the pressure melting point and incapable of exerting any shear stress on the overlying ice. The ice therefore slides freely above it, being held back only by longitudinal and lateral stresses. As all stress components are generally important around subglacial lakes, the SIA approximation is unable to account for them in a satisfactory way. Ice generally moves more like an ice shelf over large lakes, with uniform velocity. Deformational and frictional heating thus largely disappear in the ice above them. As the ice speeds up it gets drawn down by vertical flow at the edges and the ice surface tends to level above it. This effect that subglacial lakes have on the ice surface also affects the hydrological potential and it has been

hypothesized that this surface levelling has a stabilizing effect on their presence through deglaciation cycles or changes in ice configuration (Livingstone et al., 2012). They are thus likely to persist once formed, and lakes can be found in places, after reorganisation of the ice sheet geometry, where no corresponding sink in the hydrological potential can be measured.

4.3 (Lake storage capacity)

Subglacial lakes accumulate and store considerable amounts of meltwater and some estimates put the amount of stored subglacial lake water in Antarctica at around 12000-24000 km^3, equivalent to about 0.5-1m thick water layer if spread out evenly underneath the entire Antarctic Ice Sheet (Pattyn, 2008). Typical basal meltrates are on the order of a few millimetres per year and the time it takes for the ice sheet to produce the amount of stored water is thus on the order of a few hundred to a thousand years. During the last 100ka years of its existence, the Eurasian IS went through several phases of deglaciation followed by repeated regrowth until its final demise around 10k years ago. Deglaciation typically happens fast compared to growth and as we see in its final stages, the ice sheet almost completely disappeared over a period of roughly a thousand years from 13ka to 12ka (2). Such drastic changes in ice sheet geometry have profound influences on the subglacial hydrological system. Not only do basal meltrates peak during deglaciation phases, but there are also profound changes in the storage of subglacial water due to the reconfiguration of the ice sheet geometry and isostatic uplift. We see from Fig. 7 that the rate of loss in storage capacity of subglacial water can equal or surpass the amount of basal water produced during the same time. The amount of water draining from subglacial lakes can therefore drastically increase the output of subglacial water reaching the margin during deglaciation. The effect that this will have on ice sheet dynamics in general will depend on how the water is transported downstream, either in a channelized system or via a distributed system. Its effects would range from little to a potentially significant increase in average ice velocities as witnessed at Byrd Glacier in East Antarctica a decade ago Stearns et al. (2008) with faster deglaciation pursuing.

5 Conclusions

Water enhanced sliding leads to both a drop in ice volume and thickness and due to increased advection of cold ice from above and less available deformational energy, the fraction of the bed at pressure melting is reduced. Subglacial water plays an important role in initiating and maintaining ice streaming areas as well as in efficiently eroding bedrock and transporting sediment. Ice streams can only be mimicked with the shallow ice approximation and higher order physics would be needed to fully capture their dynamic behaviour. Several subglacial lakes are predicted to have existed underneath the Fennoscandian and the Barents Sea Ice sheets, some of which coincide with large surface lakes in Scandinavia at present. A considerable amount of water will have been stored in these lakes during glacial times and flushed out during deglaciation phases, potentially multiplying the amount of available subglacial water in motion. A simple thin-film water model is unable to capture the true nature of such an increase, as channel formation is excluded and all added water leads to faster sliding. The question remains, what effect such dynamic water storage in both lakes and sediment would have on ice dynamics in general and future modelling efforts will have to focus on not only more realistic models of ice and water flow but also on including dynamic storage of subglacial water.

Acknowledgements. Funding for this work came from the Research School in Arctic Marine Geology and Geophysics (AMGG) at the University of Tromsø and from the Research Council of Norway (RCN), Statoil, Det Norske ASA and BG group Norway (grant 200672) to the PetroMaks project "Glaciations in the Barents Sea area (GlaciBar)", This is also a contribution to the Centre of Excellence: Arctic Gas Hydrate, Environment and Climate (CAGE) funded by RCN (grant 223259).

References

Andersen, K. K., Svensson, A., Johnsen, S. J., Rasmussen, S. O., Bigler, M., Röthlisberger, R., Ruth, U., Siggaard-Andersen, M.-L., Steffensen, J. P., Dahl-Jensen, D., et al.: The Greenland ice core chronology 2005, 15–42ka. Part 1: Constructing the time scale, Quaternary Science Reviews, 25, 3246–3257, 2006.

Anderson, J. B., Shipp, S. S., Lowe, A. L., Wellner, J. S., and Mosola, A. B.: The Antarctic Ice Sheet during the Last Glacial Maximum and its subsequent retreat history: a review, Quaternary Science Reviews, 21, 49–70, 2002.

Andreassen, K. and Winsborrow, M.: Signature of ice streaming in Bjornoyrenna, Polar North Atlantic, through the Pleistocene and implications for ice-stream dynamics, Annals Of Glaciology, 50, 17–26, http://www.ingentaconnect.com/content/igsoc/agl/2009/00000050/00000052/art00003, 2009.

Bamber, J. L., Vaughan, D. G., and Joughin, I.: Widespread complex flow in the interior of the Antarctic ice sheet, Science, 287, 1248–1250, 2000.

Barker, S., Knorr, G., Edwards, R. L., Parrenin, F., Putnam, A. E., Skinner, L. C., Wolff, E., and Ziegler, M.: 800,000 years of abrupt climate variability, science, 334, 347–351, 2011.

Bell, R.: The role of subglacial water in ice-sheet mass balance, Nature Geoscience, 1, 297–304, 2008.

Bjarnadóttir, L. R., Winsborrow, M. C., and Andreassen, K.: Deglaciation of the central Barents Sea, Quaternary Science Reviews, 92, 208–226, 2014.

Budd, W. and Warner, R.: A computer scheme for rapid calculations of balance-flux distributions, in: International Symposium on Ice Sheet Modelling, vol. 23, pp. 21–27, 1996.

Clason, C. C., Applegate, P., and Holmlund, P.: Modelling Late Weichselian evolution of the Eurasian ice sheets forced by surface meltwater-enhanced basal sliding, Journal of Glaciology, 60, 29–40, 2014.

Dee, D., Uppala, S., Simmons, A., Berrisford, P., Poli, P., Kobayashi, S., Andrae, U., Balmaseda, M., Balsamo, G., Bauer, P., et al.: The ERA-Interim reanalysis: Configuration and performance of the data assimilation system, Quarterly Journal of the Royal Meteorological Society, 137, 553–597, 2011.

Evans, J., Dowdeswell, J. A., Ó Cofaigh, C., Benham, T. J., and Anderson, J. B.: Extent and dynamics of the West Antarctic Ice Sheet on the outer continental shelf of Pine Island Bay during the last glaciation, Marine Geology, 230, 53–72, 2006.

Flowers, G. E.: Modelling water flow under glaciers and ice sheets, Proceedings of the Royal Society of London A: Mathematical, Physical and Engineering Sciences, 471, doi:10.1098/rspa.2014.0907, 2015.

Forsström, P.-L. and Greve, R.: Simulation of the Eurasian ice sheet dynamics during the last glaciation, Global and Planetary Change, 42, 59–81, 2004.

Fricker, H., Scambos, T., Bindschadler, R., and Padman, L.: An active subglacial water system in West Antarctica mapped from space, Science, 315, 1544–1548, 2007.

Glen, J.: The creep of polycrystalline ice, Proceedings of the Royal Society of London. Series A. Mathematical and Physical Sciences, 228, 519–538, 1955.

Gray, L., Joughin, I., Tulaczyk, S., Spikes, V., Bindschadler, R., and Jezek, K.: Evidence for subglacial water transport in the West Antarctic Ice Sheet through three-dimensional satellite radar interferometry, Geophysical Research Letters, 32, n/a–n/a, doi:10.1029/2004GL021387, http://dx.doi.org/10.1029/2004GL021387, l03501, 2005.

Greve, R.: Application of a polythermal three-dimensional ice sheet model to the Greenland ice sheet: response to steady-state and transient climate scenarios, Journal of Climate, 10, 901–918, 1997.

Greve, R. and Blatter, H.: Dynamics of ice sheets and glaciers, Springer-Verlag Berlin Heidelberg, Berlin, 2009.

Johnson, J. and Fastook, J. L.: Northern Hemisphere glaciation and its sensitivity to basal melt water, Quaternary International, 95, 65–74, 2002.

Kageyama, M., Braconnot, P., Bopp, L., Caubel, A., Foujols, M.-A., Guilyardi, E., Khodri, M., Lloyd, J., Lombard, F., Mariotti, V., et al.: Mid-Holocene and Last Glacial Maximum climate simulations with the IPSL model—part I: comparing IPSL_CM5A to IPSL_CM4, Climate dynamics, 40, 2447–2468, 2013.

Kleiner, T. and Humbert, A.: Numerical simulations of major ice streams in western Dronning Maud Land, Antarctica, under wet and dry basal conditions, Journal of Glaciology, 60, 215–232, 2014.

Le Brocq, A., Payne, A., Siegert, M., and Alley, R.: A subglacial water-flow model for West Antarctica, Journal of Glaciology, 55, 879–888, 2009.

Le Brocq, A. M., Payne, A. J., and Siegert, M. J.: West Antarctic balance calculations: impact of flux-routing algorithm, smoothing algorithm and topography, Computers & geosciences, 32, 1780–1795, 2006.

Livingstone, S. J., Clark, C. D., Piotrowski, J. A., Tranter, M., Bentley, M. J., Hodson, A., Swift, D. A., and Woodward, J.: Theoretical framework and diagnostic criteria for the identification of palaeo-subglacial lakes, Quaternary Science Reviews, 53, 88–110, 2012.

Lliboutry, L.: General theory of subglacial cavitation and sliding of temperate glaciers, Journal of Glaciology, 7, 21–58, 1968.

Nye, J. and Frank, F.: Water at the bed of a glacier, in: Symposium at Cambridge 1969 - Hydrology of Glaciers), vol. 95, pp. 189–194, Cambridge England, IAHS Publishing, 1973.

Pattyn, F.: Investigating the stability of subglacial lakes with a full Stokes ice-sheet model, Journal of Glaciology, 54, 353–361, 2008.

Payne, A. and Baldwin, D.: Thermomechanical modelling of the Scandinavian ice sheet: implications for ice-stream formation, Annals of Glaciology, 28, 83–89, 1999.

Röthlisberger, H.: Water pressure in intra- and subglacial channels, Journal of Glaciology, 11, 177–203, 1972.

Saha, S., Moorthi, S., Pan, H.-L., Wu, X., Wang, J., Nadiga, S., Tripp, P., Kistler, R., Woollen, J., Behringer, D., et al.: The NCEP climate forecast system reanalysis, Bulletin of the American Meteorological Society, 91, 1015–1057, 2010.

Shreve, R.: Movement of water in glaciers, Journal of Glaciology, 11, 205–214, 1972.

Siegert, M., Dowdeswell, J., Gorman, M., and McIntyre, N.: An inventory of Antarctic sub-glacial lakes, Antarctic Science, 8, 281–286, 1996.

Siegert, M. J. and Dowdeswell, J. A.: Numerical reconstructions of the Eurasian Ice Sheet and climate during the Late Weichselian, Quaternary Science Reviews, 23, 1273–1283, 2004.

Stearns, L. A., Smith, B. E., and Hamilton, G. S.: Increased flow speed on a large East Antarctic outlet glacier caused by subglacial floods, Nature Geoscience, 1, 827–831, 2008.

Svendsen, J. I., Alexanderson, H., Astakhov, V. I., Demidov, I., Dowdeswell, J. A., Funder, S., Gataullin, V., Henriksen, M., Hjort, C., Houmark-Nielsen, M., et al.: Late Quaternary ice sheet history of northern Eurasia, Quaternary Science Reviews, 23, 1229–1271, 2004a.

Svendsen, J. I., Gataullin, V., Mangerud, J., and Polyak, L.: The glacial history of the Barents and Kara Sea region, Developments in Quaternary Sciences, 2, 369–378, 2004b.

Tulaczyk, S., Kamb, W. B., and Engelhardt, H. F.: Basal mechanics of ice stream B, West Antarctica: 1. Till mechanics, Journal of Geophysical Research B, 105, 463–481, 2000.

Uppala, S. M., Kållberg, P., Simmons, A., Andrae, U., Bechtold, V., Fiorino, M., Gibson, J., Haseler, J., Hernandez, A., Kelly, G., et al.: The ERA-40 re-analysis, Quarterly Journal of the Royal Meteorological Society, 131, 2961–3012, 2005.

Weatherall, P., Marks, K. M., Jakobsson, M., Schmitt, T., Tani, S., Arndt, J. E., Rovere, M., Chayes, D., Ferrini, V., and Wigley, R.: A new digital bathymetric model of the world's oceans, Earth and Space Science, pp. n/a–n/a, doi:10.1002/2015EA000107, http://dx.doi.org/10.1002/2015EA000107, 2015EA000107, 2015.

Weertman, J.: On the sliding of glaciers, J. Glaciol, 3, 33–38, 1957.

Weertman, J.: General theory of water flow at the base of a glacier or ice sheet, Reviews of Geophysics, 10, 287–333, doi:10.1029/RG010i001p00287, http://dx.doi.org/10.1029/RG010i001p00287, 1972.

Weertman, J.: Effect of a basal water layer on the dimensions of ice sheets, Journal of Glaciology, 6, 3–15, 2010.

Winsborrow, M. C., Andreassen, K., Corner, G. D., and Laberg, J. S.: Deglaciation of a marine-based ice sheet: Late Weichselian palaeo-ice dynamics and retreat in the southern Barents Sea reconstructed from onshore and offshore glacial geomorphology, Quaternary Science Reviews, 29, 424–442, 2010.

Wolff, E. W., Chappellaz, J., Blunier, T., Rasmussen, S. O., and Svensson, A.: Millennial-scale variability during the last glacial: The ice core record, Quaternary Science Reviews, 29, 2828–2838, 2010.